Masteroppgave

NTNU
Norges teknisk-naturvitenskapelige universitet
Fakultet for naturvitenskap
Institutt for materialteknologi

Kristian Ringheim Moe

An experimental study of bubble behaviour at liquid-liquid interfaces

Masteroppgave i MSMT
Veileder: Kristian Etienne Einarsrud
Medveileder: Varun Loomba
Juni 2022

NTNU
Kunnskap for en bedre verden

Kristian Ringheim Moe

An experimental study of bubble behaviour at liquid-liquid interfaces

Masteroppgave i MSMT
Veileder: Kristian Etienne Einarsrud
Medveileder: Varun Loomba
Juni 2022

Norges teknisk-naturvitenskapelige universitet
Fakultet for naturvitenskap
Institutt for materialteknologi

NTNU
Kunnskap for en bedre verden

Preface

This thesis is the result some random circumstances that gave me, the author, a master thesis despite having plans for another project that did not work out in the end. The work for this thesis was supposed to be performed by post doctoral researchers, but they did not have the opportunity to see it to the end. As such, I have been given the great fortune of working with an interesting project, discover phenomena that may yet have to be described by science and hopefully contribute to a more efficient society. I am grateful to my fellow students, whom I have had scientific and casual conversations with, which have increased the value of my work and been a pleasure. Several hours in the lab have been both fun and educational, especially when accompanied by my temporary co-supervisor Varun Loomba. Sergey Bublik, one of the original workers on this project, has performed both studies that supports this thesis, left us a test rig, and assembled several reports that has kick started this thesis. I am very grateful for my main supervisor, Kristian Etienne Einarsrud, for our academic discussions, as well as his great company in the small moments when he has time to waste. It is hard to overstate how much of a support Professor Einarsrud has been throughout this thesis. Finally, the report by Edrisi, Dadvar and Dabir [1] have been a cornerstone for this project and deserves a mention.

Abstract

In metal industry tapping is a process that may aerate the molten metal and liquid slag. This can contribute to transport of metal into the slag by rising metal-entrained bubbles. The goal of this thesis has been to study the behaviour of bubbles in a cold experiment with high viscosity paraffin oil stacked on water. By the use of dimensionless numbers behaviour such as entrainment, film rupture and bubble arrestation at the interface has been studied. Attempts have been made to describe the threshold values for these behaviours in such a way that it is consistent with previous work and applicable to the metal production industry. The Weber number has been determined to be one of the most promising dimensionless parameters and the threshold value is 1.0477 for film rupture. Several dimensionless parameters that is reminiscent of the Weber number are also promising. Other promising dimensionless parameters are the Capillary number divided by the Ohnesorge number, with a threshold of 1.0236. $\pi_2 \cdot Eo$ (the Eötvös number) could also be of use, with a threshold value of 4.8723e-3. Threshold values for the other phenomena could not be determined.

A water jet forming inside the bubbles as the film of water ruptures around the bubbles has been observed. This phenomenon has yet to be described in the literature to the author's knowledge.

Sammendrag

I metallindustri er tapping en prosess som kan tilføre mye luft til det smeltede metallet og flytende slagget. Dette kan medføre transport av metall inn i slagget via stigende metalldekkede bobler. Målet med denne oppgaven er å studere oppførselen til boblene i et kaldt eksperiment med høy-viskositet parafinolje stablet på vann. Ved å bruke dimensjonsløse tall har fenomener som medbringelse, film-kollaps og stansing av bobler på sjiktet mellom oljen og vannet blitt studert. Forsøk på å beskrive grenseverdiene for disse fenomenene slik at resultatene stemmer overens med tidligere arbeid og er overførbare til metallindustri har blitt gjort. Webertallet har blitt utpekt som en av de mest lovende dimensjonsløse parametererne, og grenseverdien er 1.0477 for filmkollaps. Flere dimensjonsløse parametere som minner om Webertallet virker også lovende. En annen god parameter er Kappilærtallet delt på Ohnesorgetallet, med en grenseverdi av 1.0236. $\pi_2 \cdot Eo$ (Eötvöstallet) har også vist seg å være interessant, med en grenseverdi på 4.8723e-3. Grenseverdier for de andre fenomenene kunne ikke bestemmes.

En vannstråle som ble dannet inne i boblene mens vannfilmen kollapset rundt den ble observert. Dette fenomenet er, etter forfatterens kunnskap, fortsatt ubeskrevet i litteraturen.

Contents

1 Introduction

In metal production industry tapping of the product is a common, yet surprisingly little understood procedure. It has been characterized as in a nascent stage of development, with high hopes for the coming times. New modeling and monitoring systems are expected to substantially increase our understanding of the process and facilitate safe handling [2]. An interesting phenomena occurs when tapping a submerged arc furnace in a cascade tapping procedure. As the liquids of metal and slag is drained from the oven and starts pouring into the ladles, air is drawn with the stream and into the liquids. This air then leaves the liquids as bubbles moving to the surface. Due to surface- and interfacial phenomena, these bubbles may be able to entrain metal and carry it into the slag, which floats on the metal. Some of this entrained metal is discarded.

In this thesis, a review of the acting forces on bubbles is performed. Furthermore, a set of cold experiments are performed to study the interfacial phenomena that the bubbles may exhibit. There have been similar experiments performed in the field of multi-phase flow, what makes this report somewhat unique is the use of a high viscosity paraffin oil as the upper stacked liquid. This has been chosen in order to approximate the high viscosity that are encountered in metal production slags. Although the results may not be applicable to metal industry, the results are interesting in of themselves.

2 Theory

In this section, a review of dynamics of fluid particles are compiled, both from the perspective of a single continuous phase and with stacked immiscible continuous phases. Then the material properties that are relevant to the experiments are laid out. Finally, a compilation of the concept of similitude is presented.

2.1 Bubbles and droplets

Clift, Grace and Weber have referred to bubbles and droplets as "fluid particles" [3]. As with particles in a fluid, the forces of gravity, buoyancy, and drag are highly influential on the movement of bubbles.

Gravitational forces are not necessarily very influential on bubbles in single liquid systems due to the low density of the bubble. In cases of stacked liquids a film may form around the bubble as it traverses the liquid-liquid interface, and the weight of this can be more significant. The force of gravity is expressed as in equation 1.

$$\vec{F}_g = m_p\vec{g} = \rho_p V_p \vec{g} \tag{1}$$

In this equation m is the mass of the particle, which can be expressed by V, the volume, times ρ, it's density. g is the gravitational acceleration. Subscript p denotes that the properties pertain to the a particle.

Buoyancy forces are usually the single strongest force acting on a bubble. The force is a product of weight displacement of the surrounding medium. Equation 2 describes buoyancy forces.

$$\vec{F}_B = -\rho_f V_p \vec{g} \tag{2}$$

The subscript f denotes that the property pertain to the surrounding fluid.

Drag forces are the final acting forces on simple bubbles-in-fluid-systems. Drag is a phenomenon that occurs whenever a body moves through a liquid medium. It scales linearly with the density of the surrounding medium, and with the square of the relative velocity, as presented in equation 3

$$\vec{F}_D = \frac{1}{2}\rho_f |\vec{u}_r| \vec{u}_r A_p^* C_D \tag{3}$$

Where $\vec{u}_r = \vec{u}_f - \vec{u}_p$ is the relative speed of the particle. A_p^* is the frontal area of the particle. C_D, the drag coefficient is dependent upon relative velocity, particle geometry,

size and orientation and viscosity of the fluid. These factors generally make up the Reynolds number (which will be presented later) of the particle and as such:

$$C_D = C_D(Re_p)$$

There are three contributions to the drag coefficient for fluid particles as presented in equations 4 - 6 [3]. The first of which is due to the pressure distribution around the surface of the particle, which gives rise to "form drag".

$$C_{D1} = \frac{8}{3Re}\left(\frac{2+3\kappa}{1+\kappa}\right) \tag{4}$$

In the equation above, κ is the viscosity ratio (μ_p/μ_f) between the particle and the surrounding fluid. The next contribution to the drag is from the deviatoric normal stress. One could discuss if this is more friction than drag.

$$C_{D2} = \frac{32}{3Re(1+\kappa)} \tag{5}$$

And finally the shear stresses are contributing.

$$C_{D3} = \frac{16\kappa}{Re(1+\kappa)} \tag{6}$$

In the case of gas bubbles in most liquids the shear stress contribution can be neglected due to the low viscosity ratio. The total drag coefficient is the sum of these three [3]. Alternatively, it is reported that small bubbles follows "Stoke's law" in terms of drag coefficients. It is defined as in equation 7 [3].

$$C_{Dst} = 24/Re \tag{7}$$

2.1.1 The shape of bubbles

The shape of a bubble is not always spherical. Clift, Grace and Weber [3] have defined three groups of shapes for fluid particles. "Spherical" shape is obtained if the interfacial tension forces of the bubbles are significantly higher than the inertia forces. As such this shape is normal for small bubbles with less buoyancy force acting on it. The "ellipsoidal" category have a convex and oblate interface viewed from the side. Bubbles in this category commonly undergo periodic wobbling where the shape becomes unstable. The final category is "spherical/ellipsoidal cap", where the bubbles are flat on the bottom

and looks like a cutout from a sphere on the top. Large bubbles in this category are able to entrain liquid into skirts.

The motion and shape of a bubble can be described by the following three dimensionless numbers: Reynolds, Morton and Eötvös [3]. The Reynolds number is defined as in equation 8, and can be seen as the ratio between inertia forces and viscous forces.

$$Re = \frac{\rho u_b d_b}{\mu} \tag{8}$$

where ρ and μ is the density and dynamic viscosity of the surrounding fluid respectively. u_b and d_b is the velocity and diameter of the bubble, respectively.

The Morton number is defined in equation 9 and is a measure of the rate of viscous forces to surface tension forces in a gravity field.

$$Mo = \frac{g\mu^4 \Delta\rho}{\sigma^3 \rho^2} \tag{9}$$

Here g is the gravitational acceleration, $\Delta\rho$ is the density difference between the bubble/droplet and the surrounding fluid, and σ is the surface/interfacial tension.

The Eötvos number is the ratio of bouyancy forces to interfacial tension forces and is defined in equation 10.

$$Eo = \frac{g d_b^2 \Delta\rho}{\sigma} \tag{10}$$

With these dimensionless numbers the shape regime diagram presented in in figure 1 can be interpreted.

The Weber number and the Froude number also shows up in bubble litterature. The Weber number is a measure of the inertial or drag forces of a liquid to its surface tension, and as such can describe the stability of droplet shapes. It can be defined as in equation 11 [3] [4].

$$We = \frac{u^2 \rho L}{\sigma} \tag{11}$$

Here L is a characteristic length, and the diameter of the bubble will be used when calculating this number.

Equation 12 is an expression of the Froude number. As can be seen, it is a measure of the inertial forces to the forces of gravity.

$$Fr = \frac{u}{\sqrt{gL}} \tag{12}$$

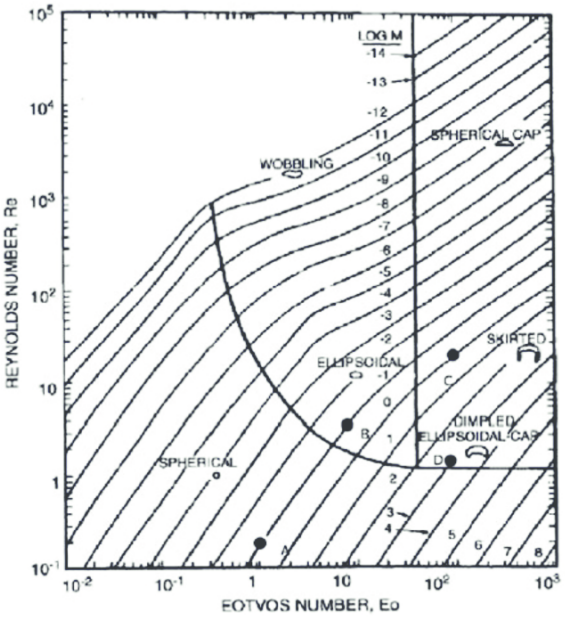

Figure 1: The shape regime as a function of Reynolds-, Eötvös- and Morton numbers

Droplets and bubbles are more complex than rigid particles, due to their soft nature and inherent fluid properties. One of the complications is the interfacial tension that tries to minimize the interface area. Furthermore as a bubble moves through a liquid, the gas in the bubbles is free to flow too, and thus the viscosity becomes relevant [3]. In figure 2 the internal flow of a water droplet in castor oil can be seen.

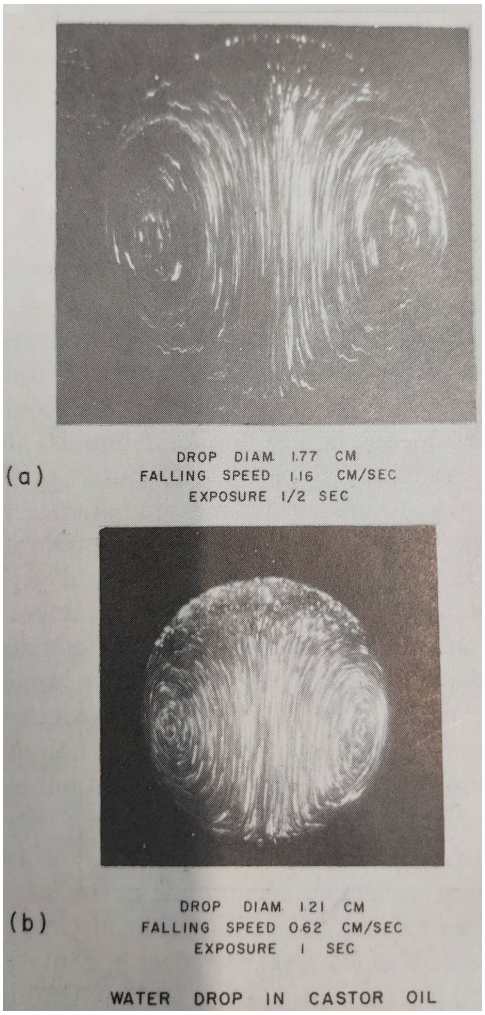

Figure 2: The internal flow of two droplets of water descending in castor oil [3].

As seen in the figure above, the internal motion of fluid particles is complex. Notice that the side that is oriented away from the direction of travel (which in this case is downwards) has a slower circulation than the rest of the bubble. This leads to an accumulation of surfactants in this part of the particle [3].

The diameter of the bubbles that are produced can be described by equation 13 [4].

$$d_b = \left(\frac{6 d_n \sigma}{\rho g} \right)^{1/3} \tag{13}$$

In this equation d_b represents the bubble diameter and d_n is the nozzle diameter. The relevance of this is mainly for reproduceability of larger bubble sizes.

2.1.2 Terminal velocity

Terminal velocity is reached when the forces acting on the bubble are in equilibrium. The forces of gravity, buoyancy and drag as presented in equations 1, 2 and 3 are the most important ones. As such, it is clear that properties of the fluid, like density and viscosity are of importance. The shape of the bubble affects the drag, and thus the surface tension between the bubble and liquid must also be considered. In the realm of bubbles, the viscosity ratio is also of interest. For air in water, this ratio is very small, and as such there is little resistance to internal circulation in the bubble and surfactants become highly influential [3]. The terminal velocity for bubbles in surfactant contaminated systems can be approximated by equation 14 below. This equation was empirically found and developed by several scientists, but the most famous contributer was Johnson and Braida [3].

$$U_T = \frac{\mu}{\rho d_e} Mo^{-0.149}(J - 0.857) \tag{14}$$

Where μ, ρ and d_e is the viscosity and density of the liquid and the equivalent diameter of the bubble respectively. Mo is the Morton number and J is a dimensionless group that takes the form as in equations 15 or 16.

$$J = 0.94H^{0.757} \qquad (2 < H \leq 59.3) \tag{15}$$

$$J = 3.42H^{0.441} \qquad (H > 59.3) \tag{16}$$

Where H is a function of the Eötvös and Morton numbers and the viscosity ratio of the bubble in the liquid. It takes the form as in equation 17.

$$H = \frac{4}{3} Eo \cdot Mo^{-0.149} \left(\frac{\mu}{\mu_l}\right)^{-0.14} \tag{17}$$

Where μ_l is the dynamic viscosity of the liquid. This correlation needs to have the following criteria met [3].

$$Mo < 10^{-3}, \qquad Eo < 40, \qquad Re > 0.1$$

2.2 Bubbles rising through an interface between immiscible stacked liquids

When tapping a melt with slag from a crucible into a ladle, a lot of air is drawn with the stream into the metal. This air escapes the ladle as bubbles moving from the metal (heavy liquid) and into the slag (light liquid).

Rozario et al. [5] has found that the terminal velocity of the bubbles rising in the light phase decreases with the viscosity of the phase. They also found similar influence by the ratio of viscosity to the density difference between the light and the heavy phase. Thus they seem to have confirmed that the flow surrounding the bubble is largely Newtonian and influenced by viscous forces.

2.2.1 Rate of drainage

The rate of drainage is the speed by which the heavy phase leaves the bubble as it rises through the light phase. Rozario et al. [5] found that the rate of drainage is primarily dependent upon the buoyancy factor ($\Delta\rho$) between the two phases. Furthermore they also found a dependency upon viscosity and interfacial tension, which was especially clear when taking the buoyancy ratio ($\Delta\rho$) and viscosity ratio (μ_1/μ_2) into account. Subscript 1 denotes the light liquid, while subscript 2 denotes the heavy liquid. With an experiment with high viscosity castor oil, the drainage of the heavy phase (water) was found to be faster due to the higher viscosity of the oil [6].

2.2.2 Satellite formation

When a bubble is passing an immiscible interface there is a possibility of ejecting a satellite of the bubble material in the opposite direction of travel. The precursor for this is that the bubble has enough size to pass the interface, but not enough to entrain heavy liquid and that the interface is convex [1], [7].

2.2.3 Passing the liquid-liquid interface and heavy phase entrainment

Greene et al. have studied the conditions under which bubbles will pass an interface of stacked liquids. Equation 18 describes the minimum volume needed to pass the interface [8]. Subscript b denotes the bubble phase.

$$V_b > \left(\frac{3.9\sigma_{12}}{(\rho_1 - \rho_b)g} \right)^{\frac{3}{2}} \tag{18}$$

Using the equation above and modifying it to take into consideration the film formation around the bubble when passing the interface an expression for the entrainment was found. Equation 19 describes the minimum volume a bubble will need in order to entrain heavy liquid and draw it into the light liquid [8].

$$V_b > \left(\frac{2 \cdot 3.9\sigma_{12}}{(3\rho_1 - 2\rho_b - \rho_2)g} \right)^{\frac{3}{2}} \tag{19}$$

2.2.4 Film rupture

Film rupture is the phenomenon that occurs when the heavy liquid leaves the rising bubble in the light liquid. The three phase contact line (TPCL) forms shortly after the film ruptures. The film may be dispersed into smaller droplets and the number and sizes of these droplets depends on the interfacial tension. The higher the interfacial tension, the larger the droplets [1]. Alternatively the heavy phase may leave as a single large droplet behind the bubble. As reported by Kobayashi [9]: Conochie and Robertson introduced three parameters to indicate the stability of the entrained film, they are as follows in equation 20 - 22:

$$X = \sigma_{12}/\sigma_t \tag{20}$$

$$Y = \sigma_{2b}/\sigma_t \tag{21}$$

$$Z = \sigma_{1b}/\sigma_t \tag{22}$$

Subscript b denotes the bubble phase. In these equations "σ_t" is the total interfacial tension presented in equation 23.

$$\sigma_t = \sigma_{12} + \sigma_{2b} + \sigma_{1b} \tag{23}$$

The stable states were predicted as follows:

- Film for Z $>$ 0.5
- Dispersion for Y $>$ 0.5
- Flotation for Z $<$ 0.5, Y $<$ 0.5 and X $<$ Y

2.2.5 Thresholds of bubble behaviour

The dimensionless values of the bubble experiments can be used to find thresholds for the their specific behaviour. Heavy liquid film-rupture around the bubble, the penetration of the interface and the satellite formation are of interest here. In figure 3 an illustration of a bubble passing an interface, entraining heavy phase, and draining of the heavy phase is visible. The heavy phase will drain off the bubble until a thin film is left behind or the film ruptures.

Figure 3: A bubble, passing an interface and entraining the heavy phase [1].

Edrisi et al. [1] introduced several dimensionless groups that they used to describe the threshold values for the former two phenomena. The dimensionless groups are presented in equations 24 to 26.

$$\pi_1 = \frac{\sigma_{12}}{(\rho_2 - \rho_b)gD^2} \tag{24}$$

This is a measure of the ratio of interfacial tension to bouyant forces acting on the rising bubble in the heavy liquid. σ_{12} is the interfacial tension force between specie 1 (light liquid), and specie 2 (heavy liquid). Edrisi et al. [1] has found the threshold limits

of bubble bouncing on the interface (no penetration) to be 0.17585 for this measure. They also expressed the heavy film rupture on the bubble rising in the light liquid to be 0.02057 [1].

$$\pi_2 = \frac{\mu_2}{(\rho_2 - \rho_b)\sqrt{gD^3}} \tag{25}$$

This is defined as the ratio of viscous forces to buoyant force acting on the bubble rising in heavy liquid. The bubble bouncing on the interface threshold for this value is 0.19909. The heavy liquid film rupture starts at 0.00796 for this value according to Edrisi et al [1].

$$\pi_3 = \frac{\rho_1 - \rho_b}{\rho_2 - \rho_b} \tag{26}$$

This parameter is the ratio of net upward buoyancy to net downward gravitational forces acting on bubble and entrained liquid. The threshold value for this parameter was only found for bouncing on interface phenomena, at 1.93721 [1].

In addition to these relatively obscure dimensionless groups there are some more well known groups that take in the relevant properties of the experiment. The following numbers are used in the analysis of the bubble behaviours. The Archimedes number is a measure of the gravitational forces to viscous forces acting on a body in a fluid. It takes the form as in equation 27.

$$Ar = \frac{gL^3\rho_l(\rho_b - \rho_l)}{\mu^2} \tag{27}$$

Here ρ_b is the density of the submerged body, ρ_l is the density of the liquid, and L is a characteristic length of the body.

The Capillary number represents the effect of viscous drag to surface tension acting between two fluids in relative motion. It is presented in equation 28.

$$Ca = \frac{\mu u}{\sigma} \tag{28}$$

The Ohnesorge number is a measure of viscous forces to inertial and interfacial tension forces. In addition to the form in equation 29, it can also be expressed as the square root of the Weber number (equation 11) divided by the Reynolds number (equation 8).

$$Oh = \frac{\mu}{\sqrt{\rho\sigma L}} \tag{29}$$

The Galilei number quantifies the gravity forces to the viscous forces in the system and takes the form as in equation 30.

$$Ga = \frac{gL^3}{\nu^2} \tag{30}$$

where ν is the kinematic viscosity.

The Laplace number is a measure of surface tension to momentum and dissipation. It can be expressed as a ratio of the square of the Reynolds number to the Weber number. It is presented in equation 31.

$$La = \frac{\sigma\rho L}{\mu^2} \tag{31}$$

As is clear, the Ohnesorge number and the Laplace number are related, as $La = Oh^{-2}$.

2.3 Relevant fluid properties

In this section the properties of fluids that are applicable to the experiments are presented.

2.3.1 Surface tension

Surface tension is a phenomena where the surface of a fluid acts somewhat as though there was an elastic film stretching around it, tending towards a spherical shape if no other forces act on it. Exactly how this phenomena occurs has been subject to long discussions, and in some cases even been completely dismissed as a work of fiction [10]. Surface tension stems from the fact that in a liquid, the surface layer of molecules have different forces acting on them compared to a molecule placed within the bulk. This also gives rise to interfacial tension when liquids are not miscible [10].

Edrisi et al. [1] proposed a method of determining the interfacial tension by the smallest bubble volume that could pass the interface of two stacked liquids. The forces of bouyancy and the inertia of the bubble are the contributors to the penetration. They

proposed equation 32 presented below.

$$\sigma = \frac{V_b^{2/3}((\rho_2 - \rho_b)g + \rho_2 \frac{u_t - u_n}{\Delta t})}{3.9} \approx \frac{V_b^{2/3}\rho_2 g}{3.9} \tag{32}$$

In this equation, V_b denotes the smallest bubble volume that can penetrate the interface. ρ_2 is the density of the heavy liquid, while ρ_b is the density of the bubble. u_t is the terminal velocity of the bubble before the interface is deformed by the rising bubble. When the bubble has hit the interface, it usually draws out a tail of the heavy liquid into the lighter. u_n is the velocity of the bubble during the initiation of necking of this column [1]. If the density and inertia of the bubble is neglected (as a consequence of these sizes being very small) the expression on the right of the approximate sign is obtained.

When the bubble has reached the liquid-liquid interface, three phenomena may occur: the bubble passes the interface, the bubble does not pass the interface, or the bubble may rest on the interface for a moment before passing. Rozario and Basu has found that the lower the interfacial tension, the lower the residence time of the bubbles at the interface [6].

As this thesis aims to describe the interactions of bubbles passing two liquids, it is a three phase fluid problem. Therefore, studies of compound drops [sic] are of interest. A compound or multiphase drop system is a set of drops of two or more immiscible fluids that surrounded by a mutually immiscible fluid. An illustration is presented in figure 4.

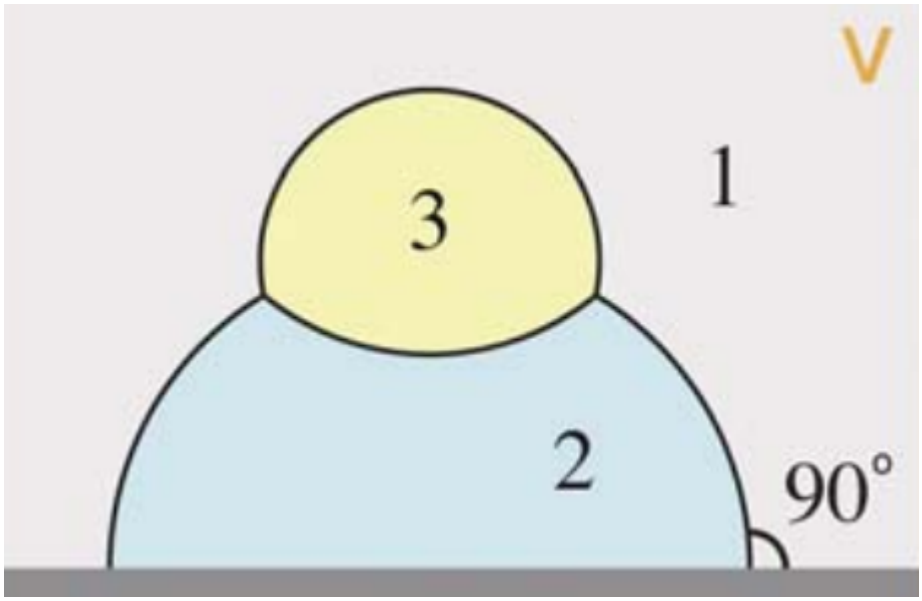

Figure 4: A compound drop system. Phases 1, 2 and 3 are three mutually immiscible liquids [11].

A three phase contact line may form between three such fluids under certain conditions. In the case of three mutually immiscible fluids the surface tension forces need to be such that the triangular inequality in equation 33 is satisfied [11].

$$\sigma_{12} < \sigma_{23} + \sigma_{31} \tag{33}$$

In this equation the subscript 12 denotes the surrounding fluid (1) to one of the compound fluids (2). If the tension between the surrounding fluid to the lightest compound is more than the sum of the two others, the three phase contact line will not be formed on a sessile compound drop system [11]. Both Neeson et al. [11] and Edrisi et al. [1] outlines the conditions with illustrative pictures and experimental results for sessile drops and rising bubbles respectively. The conditions for which a rising bubble will experience a three phase contact line is more complicated, as drag and gravity plays an important role in drawing out any surrounding film as the pressure inside the film rises due to the movement [12] [1] and gravity acts on the heavy phase film as well. The three fluids have different interfacial tensions to each other, and as such will stretch and deform accordingly. Pannacci et al [13] introduced the "spreading parameter", which is presented in equation 34.

$$S_b = \sigma_{12} - (\sigma_{b1} + \sigma_{b2}) \tag{34}$$

A positive spreading parameter for the bubble implies it will be flat and drawn and resting between the interface while a negative spreading parameter implies the bubble will be more spherical. The spreading parameter can be calculated for each phase. With a positive spreading parameter for a liquid, the TPCL wil be on the interface between the stacked liquids and the bubble will be inside the liquid with negative spreading parameter if at rest [1] [11]. Chevrier and Cramb [14] found that the film drainage increase with interfacial tension by studying the effect of added surfactants.

2.3.2 Surfactants

Surfactants are a group of chemicals that decrease the surface tension of liquids. A surfactant has one end that has very little attraction to the solvent, known as the lyophobic group, and one that has a high attraction to the solvent, known as the lyophilic group. As the amphipathic structure is usually not entirely soluble in a liquid, it is forced to the interfaces. Considering a system of more than one phase there will be a more continuous transition between the two fluid's properties, and the surface tension is drastically reduced [15]. In addition to decreasing the surface tension, they also tend to make the interface rigid and as such reduce internal motion of fluid particles. Therefore the terminal velocity of a bubble or droplet usually decreases. This effect is most prominent for low viscosity ratio between the bubble (denoted "b") and the surrounding fluid (μ_b/μ). Bubbles with an equivalent diameter of 0.5 - 10 mm are also most affected. The higher the surface tension of the system the more influenced it is by surfactants [3]. The magnitude of surface activity of surfactants is defined as the change in the system's surface tension per unit content of solute surfactant [16].

2.3.3 Viscosity

> Big whirls have little whirls,
> That feed on their velocity;
> And little whirls have lesser whirls,
> And so on to viscosity.
> - Lewis Fry Richardson

As indicated in the observations of Lewis Fry Richardson, viscosity is a mechanism that atrophies a system of its kinetic energy, like friction. Viscosity is defined as "a quantitative measure of a fluid's resistance to flow" [17]. It is an inherent property

of a fluid, and as such, a multiphase flow problem will contain complex inherent flow resistances. Viscosity can be expressed as dynamic viscosity, with the unit $Pa \cdot s$. Alternatively one can use kinematic viscosity, which is dynamic viscosity divided by the density of the fluid, with the unit m^2/s.

In industrial applications of metal production, the metals usually have a viscosity in the $mPa \cdot s$ range. Iron, for example has a viscosity of 2.92 $mPa \cdot s$ at 2000 degrees. Many slags are close to 0.1 $Pa \cdot s$ in this temperature, and as such they are about two orders of magnitude more flow resistant than metals. Furthermore, the viscosities of slags are heavily temperature dependent [16].

Chevrier and Cramb [14] found that the rest time at the interface for bubbles were dependent upon the kinematic viscosity of the upper stacked liquid, the higher the viscosity the longer the rest time. They propose that this is due to the rate of film drainage, which is more rapid when the viscosity is lower. They also conclude that the viscosity of the upper liquid layer is the strongest factor influencing the separation of particles at the liquid-liquid interface.

2.3.4 The Buckingham Pi theorem

The Buckingham pi theorem states that given a physically meaningful equation, the equation can be written as a set of dimensionless groups. The number of groups equals the number of variables minus the amount of physical dimensions (base SI-units). The theorem does not give any indication on what groups are fitting for the problem, nor the form of the function [18]. Thus far, the properties of relevance are density, surface- and interfacial tension, and viscosity for the phases in addition to the size and velocity of the bubble. These properties are all some variations of the three physical dimensions kg, m and s, and as such

2.4 Similitude

The concept of similitude is of importance to this thesis. If two conditions have similitude (in the relevant properties) they will act similarly. This concept is of crucial importance to many small scale experiments. However, small and low temperature models have been hard to apply to large scale metal casting processes. Shortcomings stems from the large difference namely in scale, density, viscosity and surface tension [19]. As this has been problematic in the past, the similitude of the model liquids will

be presented expressed by a similitude parameter, which will be introduced shortly.

This thesis will try to present the results in such a manner that they are dimensionless, and that their direct similitude is obvious. The relevant properties of bubbles and flow have recently been studied by Tsukaguchi et al. [4]. The dimensionless parameters that are of most importance for bubbles and droplets are as follows: Froude-, Reynolds-, Weber- and Eotvos/Bond-number. Tsukaguchi et al. expressed the scale ratio on the Reynolds and Froude numbers as in equation 35.

$$\lambda_{FR} = \left(\frac{\nu}{\nu_0}\right)^{2/3} \tag{35}$$

Where ν is the kinematic viscosity. This scale ratio was found by substituting the length in the Froude number with the characteristic length and expressing the velocity similarly and substituting this into the Reynolds number. As such a physical setup with fluids that has the same scale ratio can be applied to another set of fluids [4]. Similarly the scale ratio for the Weber and Froude number has been found to be as expressed in equation 36.

$$\lambda_{FW} = \left(\frac{\sigma\rho_0}{\sigma_0\rho}\right)^{1/2} \tag{36}$$

Tsukaguchi et al. [4] then presents the S-parameter, which is a measure of how much similitude there is of this multiple of dimensionless numbers. The S-number or similitude of multiple dimensionless numbers (SMDN)-parameter is presented in equation 37.

$$\frac{\sigma^{1/2}}{\nu^{2/3}\rho^{1/2}} = \frac{\sigma_0^{1/2}}{\nu_0^{2/3}\rho_0^{1/2}} \tag{37}$$

If the liquid of the model and the liquid of the real application has the same values in this regard, the model results should be immediately applicable. However, with these functions of similitude the only acting forces permitted are the inertial, gravitational, viscous and surface tension forces and the liquid must be newtonian and incompressible. As can be seen in the equation, surfactants would lower the SMDN number of a system. With these sets of equations the products this thesis is trying to facilitate the production of can be calculated.

3 Methodology

Here the methods, materials and equipment are explained. Software used to evaluate the experiments are laid out as well.

3.1 Experimental setup

The test rig was inspired by the experiments of Edrisi et al. [1]. A tall acrylic box serves as the bubble rise chamber. There are two boxes connected to this at different heights for containing water and oil. The rig is presented in figure 5. The inlet to the rise chamber was challenging to construct due to bubbles adhering to the walls of the tubes. A 1 inch PVC tube inlet was fastened to the bottom of the chamber, through which a 15 mm tube going to the syringes protrudes somewhat. At the front a Sony RX10iv camera was placed to capture the bubble behaviour. Untreated tap water is used as the heavy liquid in the bottom. The interfacial tension between the oil and the water has been determined by optical tensiometry by pendant droplet shape analysis. All relevant properties are to be found in table 1. The height of the water phase was 9 cm, the height of the oil was 7 cm, and the temperature was 22 degrees Celsius for all experiments with water and oil. A set of single liquid (water) experiments was also performed in order to assure that the test rig could perform to the standards needed and that the results were reproducible.

Table 1: Properties of the fluids of the experiments.

	Water	Oil	Air
Density [kg/m^3]	998	855	1.20
Viscosity [mPa s]	1.002	56.7	1.825e-2
Surface tension [mN/m]	72.8	30.75	
Interfacial tension [mN/m]	37.3		
Spreading parameter [mN/m]	-0.07935	0.004750	-0.06625

The spreading parameters for each phase is shown. The positive spreading parameter of the oil is implying that the TPCL is drawn down on the bubble surface and that the bubble will eventually enter the light liquid. Also note the low density difference between the oil and the water. The bubbles that are trapped on the interface is thus suspended in the oil, and not in the water, which is possible to see in figure 11.

The similitude of multiple dimensionless numbers (Froude-, Reynolds-, Weber- and Eötvös numbers) as expressed by Tsukaguchi et al. in equation 37 is presented in table 2. The SMDN range is a function of the temperature, since the properties that make up the number are affected by it.

Table 2: The SMDN values of the fluids used in the experiments.

Fluid	SMDN slope, surface tension	Range [f(T)]	SMDN slope, interfacial tension
Water	85.2	64-205 *	60.97
Oil	3.66	not tested	4.03

* the values are as calculated by Tsukaguchi et al. [4].

The camera had a recording setting of 960 fps and saves the video in 24 fps, thereby getting a 40x slow motion recording of the action. In all experiments the camera was placed in the same position, about half a meter from the test chamber. The entire setup is as illustrated in figure 5.

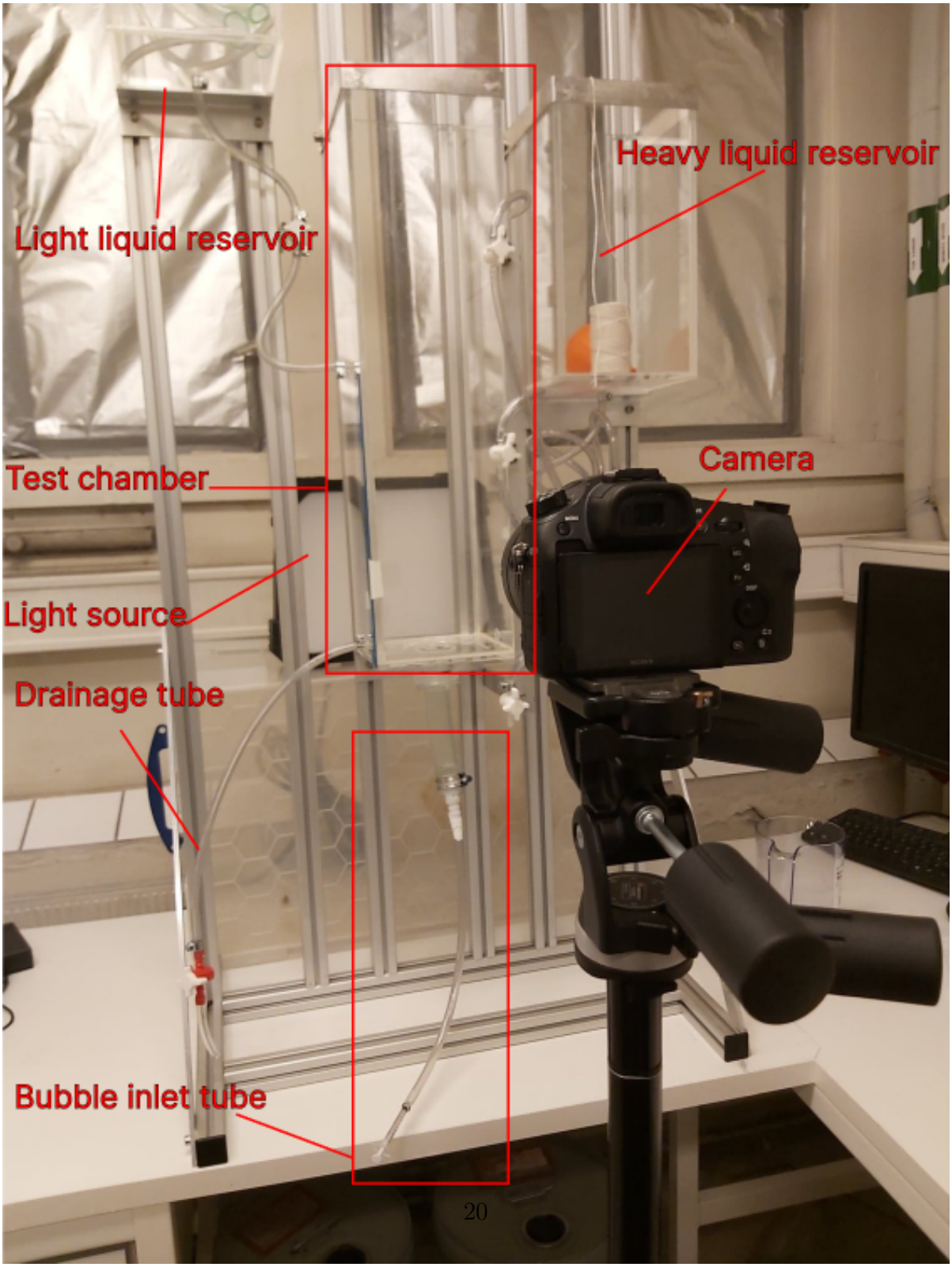

Figure 5: The test rig with the camera

There was some attempts at adding food coloring to the water in order to get more distinct edges in the image, and thus ease the automated imaging processing. This seems to have added a lot of surfactants that negatively impacted the experiments. This is discussed later.

3.2 Experiments

Several experiments were performed to test the equipment and establish the range of experiments that could be performed. Thus the range of bubble volume was established, the functionality of the equipment was assessed, and some trial and error in image analysis was performed. The results from these experiments will be glossed over in the Results section.

The bubble range that has been studied has been in the range of 0.2 ml to 0.05 ml. The 0.2 ml was the maximum volume that could be studied without the bubbles breaking apart when entering the chamber. In order to get a larger range of sizes a larger range of inlet nozzle sizes would be needed. 7 parallels has been run without zoom in order to study the trajectory and the influence the high viscosity oil has on the entrained water. A set of close up films has also been made in order to study the drainage and film ruptures when the bubbles pass the interface. The videos of the experiments can be found here `https://www.youtube.com/playlist?list=PL5dgkn-i55F9s633ieywrZ0FkNbBUK9Rd`. There was one attempt at adding food coloring to enhance the contrast of the two phases so that analysis would be smoother. The coloring seemed to contain large amounts of surfactants, and as such could not be compared to the cases with "clean" tapwater.

3.2.1 Calculation of drag

Since the bubble sizes studied here are in the borderlands of "small" and "medium" sized, the drag forces will be calculated with both Stokes Law of drag coefficient from equation 7 and with the three contributions from equations 4 - 6. The results are based on the terminal velocities of the bubbles in the water and in the oil.

3.3 Analysis of video

The videos of the bubbles were first processed in FFMPEG into single images before being analyzed as a stack in ImageJ [20]. The steps will be laid out in the following list,

and the effect they have on the images is presented in figure 6.

1: Convert captured image to 8-bit for easier processing. Enhance contrast to make edges easier to find.

2: Use "Find edges" tool to define the outlines of the bubble. Then smooth out the edges so that thresholding is less prone to discard an image where the edge is incomplete.

3: Threshold the image so that everything with bright pixels are kept, while everything below a certain pixel brightness is discarded.

4: Use "Analyze particles" tool to obtain the position of the bubble's center mass for each image. This is the value that has been tracked.

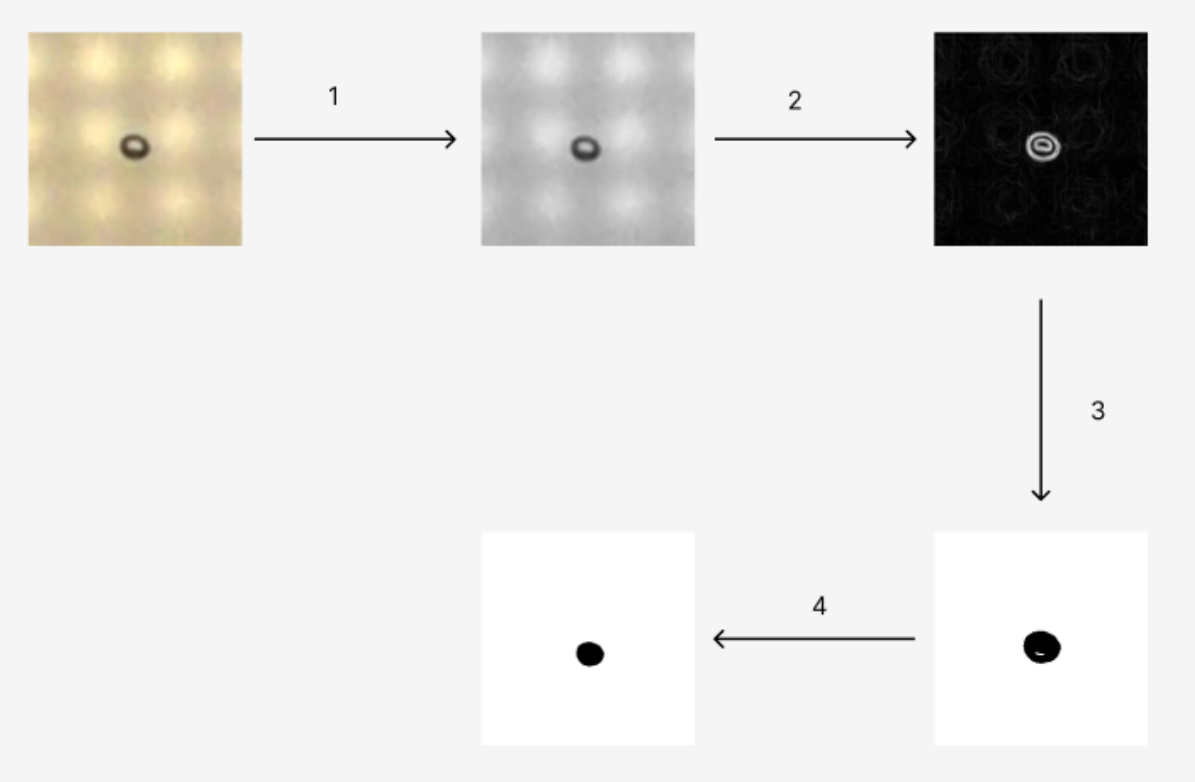

Figure 6: The effects of the processing steps from the list above.

3.4 Finding threshold values

The threshold values for the bubble behaviour has been studied by a set of dimensionless parameters that has been suspected to be somewhat representative of all forces and effects on the bubble, as defined in section 2.2.5, and in 2.1.1. These parameters are checked one to one for the experiment performed for this thesis to the experiments of Edrisi et al. [1]. The goal is to find some similarity between the results for film rupture in the two different sets of experiments. All the previously introduced dimensionless numbers, as well as the numbers introduced in section 3.4.1 have been studied and compared for the experiments. The values are rarely in the same order of magnitude though, and as such the dimensionless parameters have also been laid out in a 2D matrix where the parameters are multiplied with- or divided upon each other for one experiment. Then the values from one experiment is checked against the other experiment similarity in the dimensionless parameters. The given data has not been very easy to study due to a lack of velocity data from previous work, and a guesstimation of the terminal velocity of the bubble by the use of equation 14 and by the velocity of the other bubbles in the system has been performed. In order to properly threshold the behaviours of film rupture it is important that further research into this topic is performed, with a varied set of fluids and a detailed data representation. Some dimensionless parameters have been created by analyzing the properties that seem to be of importance.

3.4.1 New dimensionless parameters

When assessing the forces acting on the entrained water it should be possible to conclude on a set of properties that influence the film rupture. The properties pertaining to drag has been identified as the velocity of the bubble, bubble diameter and the viscosity of the oil. The properties of bubble density and -diameter and oil density has been identified as the properties pertaining to bubble bouyancy, and similarly for the gravitational force on the bubble (excluding the oil density). The interfacial tension is the property that governs the forces enacted on the entrained water that leads to contraction. The influence of gravity on the entrained water can be expressed by the volume of the thin film around the bubble and the density of water. Similarly the entrained water has some buoyancy. Considering all the forces that are acting on the bubble during its travels yields the equation presented in equation 38.

$$F_{tot} = F_D + F_{\sigma_{12}} + F_{g_2} + F_{g_b} - F_{B_b} - F_{B_2} \tag{38}$$

These force contributions have the following properties of importance:

- u_r: relative velocity of bubble.
- μ_1: viscosity of the oil.
- d_b: diameter of bubble.
- ρ_2, ρ_1 and ρ_b: Density of water, oil and bubble.
- σ_{12} Interfacial tension between water and oil.

All these properties are some variations of the physical dimensions kg, m and s, and thus the Buckingham Pi theorem states that four dimensionless groups can be used to describe this problem, given a relevant and meaningful equation.

A set of 5 additional dimensionless parameters have been introduced. To determine whether they are suitable to describe the behaviour, the trial and error approach with the cross examination script is employed. The parameters are as presented in equation 39 - 43.

$$\pi_4 = \frac{\mu_1}{(\rho_1 - \rho_b)\sqrt{g d_b^3}} \tag{39}$$

This parameter is equal to π_2 (equation 25 introduced by Edrisi et al. [1]. The only difference is that the viscosity and density of the light liquid is used instead of the heavy liquid. This parameter is further discussed in the discussion section.

$$\pi_5 = \pi_4 \cdot \pi_2 \tag{40}$$

This number thus represents the same forces acting on the bubble in the heavy liquid phase and the light liquid phase.

$$\pi_6 = \frac{\pi_4 \pi_1}{\pi_2} \tag{41}$$

The equation above is meant to reveal interactions between multiple dimensionless parameters in the 2D matrix analysis.

$$\pi_7 = \frac{\mu_1 \sigma_{12}}{\rho_1^2 v^3 d_b^2} \tag{42}$$

This number is a ratio between the viscous forces and the interfacial tension forces to the velocity and diameter of the bubble.

$$\pi_8 = \frac{\rho_1^2 g d_b^3 + \rho_1 \sigma_{12} d_b}{\mu_1^2} \tag{43}$$

π_8 is a measure of the pressure exerted by the light liquid and the interfacial tension to the viscosity of the light liquid. It is somewhat reminiscent of the Archimedes number.

With the results obtained in tables 5 and 4, the parameters with the lowest margin variance was collected and re ran through the comparison script. This was done in order to see if there were additional parameters that could be influential on the film rupture phenomena. $\pi_9 - \pi_{14}$ is presented in equations 45 - 49 below.

$$\pi_9 = \pi_3 / Fr \tag{44}$$

$$\pi_{10} = Ar / Ga \tag{45}$$

$$\pi_{11} = Ca / Oh \tag{46}$$

$$\pi_{12} = \pi_7 / Oh \tag{47}$$

$$\pi_{13} = \pi_7 / Ca \tag{48}$$

$$\pi_{14} = Eo \cdot \pi_2 \tag{49}$$

4 Results

In this section the results of all experiments are presented. Firstly the single liquid experiments and what they imply for the rest of the experiments are presented.

4.1 Single liquid

With the single liquid (only water) experiments the range of bubble sizes that could be reliably reproduced was determined to be 0.05, 0.10, 0.15 and 0.20 ml. The reason for this distribution was that the syringe had a volume of 0.5 ml, with markings every 0.05 ml. The upper limit was due to the bubbles splitting up in the nozzle with a larger volume than 0.20 ml.

The velocity of the bubbles was also assessed to determine the repeatability of the experiments. Some experiments had distinctly different velocity than others. However, after seven parallels these two outlier experiments were mostly within the 95% confidence interval. The lowest average speed was 175 mm/s, and the highest was 225. As seen in figure 7, the average speed is usually around 200 mm/s.

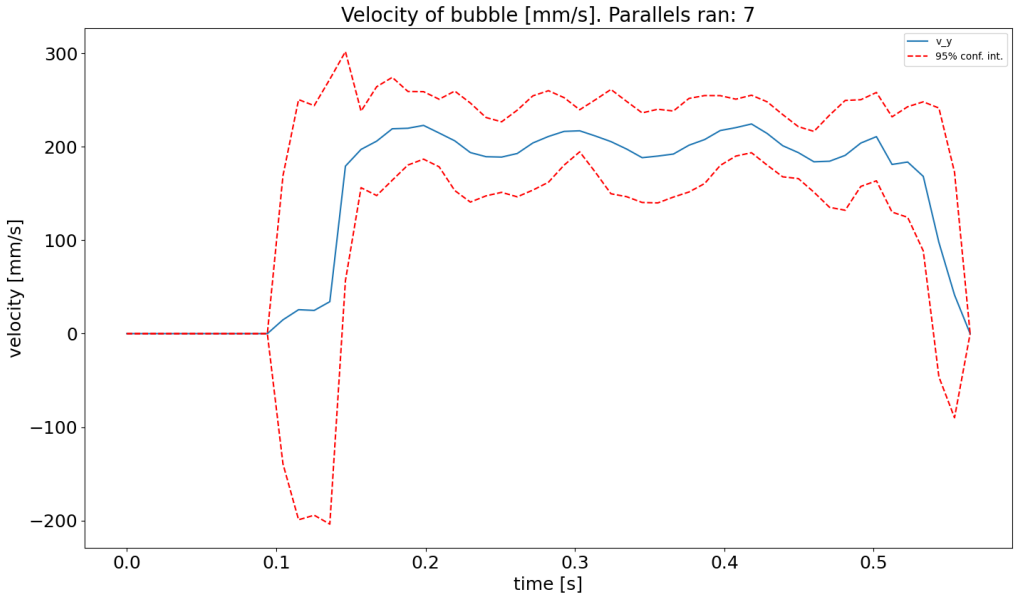

Figure 7: Gliding average (resolution = 1/10) velocities of the single liquid experiments (0.05 ml).

In the figure above, the blue line represents the average upwards velocity of the seven parallels as the bubble is rising. The red lines illustrates the 95% confidence interval in the velocities, determined by Student T distribution.

4.2 Stacked liquids

When the oil is stacked on top of the water, several changes to the bubble behaviour is observed. Additionally, the interfacial phenomena becomes important.

4.2.1 Velocity of bubbles

The terminal velocity of the bubbles are relatively high in this set of experiments, reaching almost 300 mm/s before stabilizing around 200 mm/s. The velocity quickly stabilizes after leaving the entrance nozzle to the test chamber. The raw velocity data of a 0.10 ml bubble is presented in figure 8. The absence of data points in the middle is due to the bubble not being recognized in the transition from water to oil in the test chamber. The

blue line represents the upwards velocity while the orange line represents the velocity from side to side.

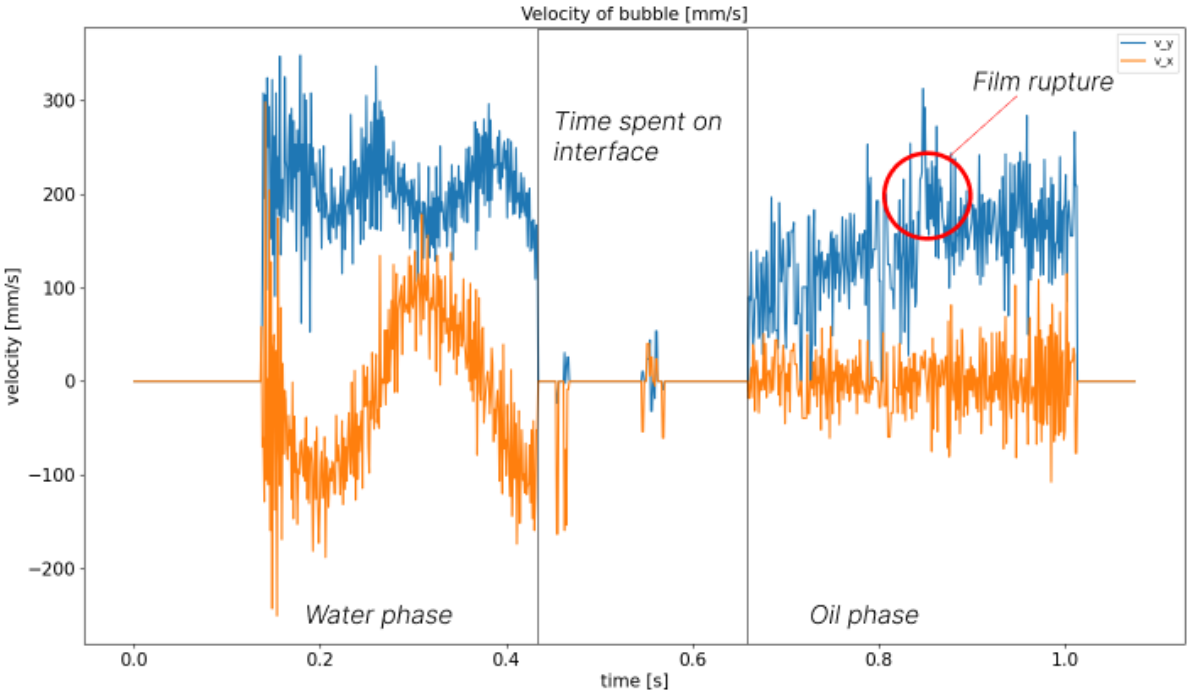

Figure 8: Raw data of velocity of a 0.10 ml bubble through first water, then oil.

As is clear from the graph, the passage to the oil layer significantly dampens the wobbling motions. This is as expected when considering the Reynolds number, which goes from between 900 - 1600 for bubbles in the water to between 10 - 20 in the oil. The upwards velocity after the bubble passes the interface is steadily rising until a sudden spike happens. In this case the spike was due to the entrained water going from a uniform distribution around the spherical bubble to mainly being a trailing tail on a flat capped bubble. The top of the bubble does not change velocity, but the bottom moves up and the bubble squeezes outwards to obtain the ellipsoidal shapes, and thus a rapid shift in center mass is observed, which gives rise to the spike. Although a different bubble size and at a different point in time, a similar behaviour can be seen in figure 11. This sudden increase in velocity is also visible in the position graph of the bubble, which is presented in figure 9.

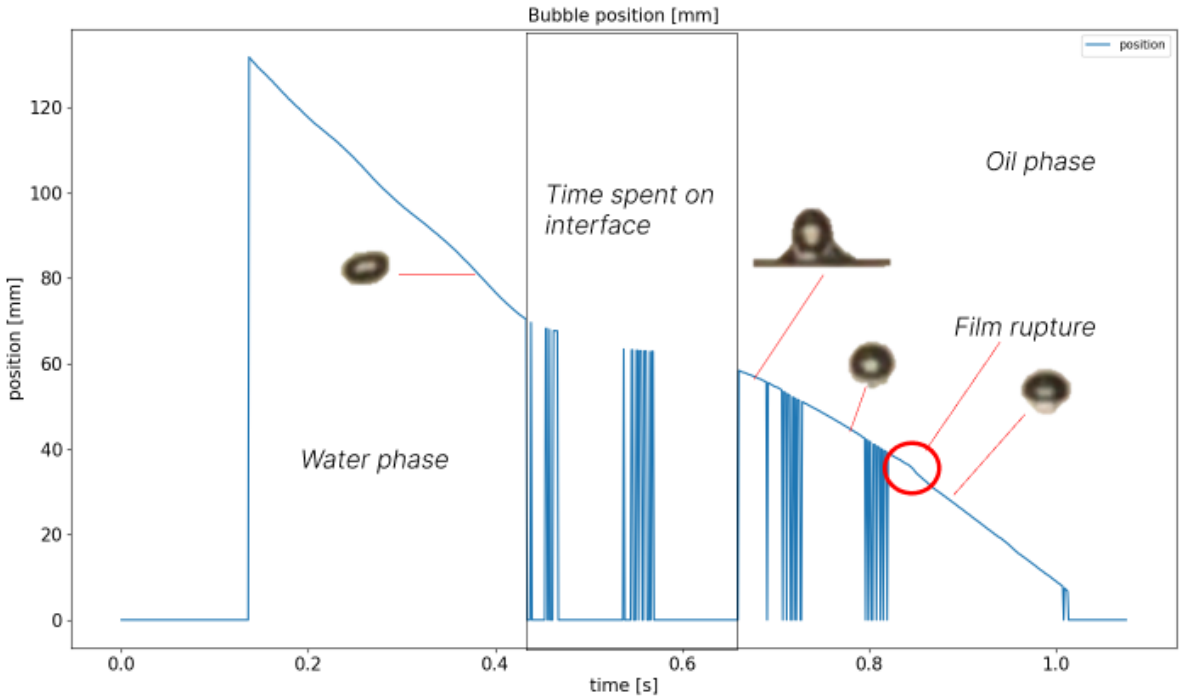

Figure 9: Position of bubble over time. The 0-value of the axis is the top of the oil surface.

Here, the sudden slope change at around 0.83 seconds is the point where the entrained water formed a tail. Upon further inspection this seems to be the point where the TPCL forms, and the water film ruptures. In subsection 4.2.3 the observations of the drainage and film rupture phenomena are presented in more detail.

The path of this bubble is tracked and presented in figure 10.

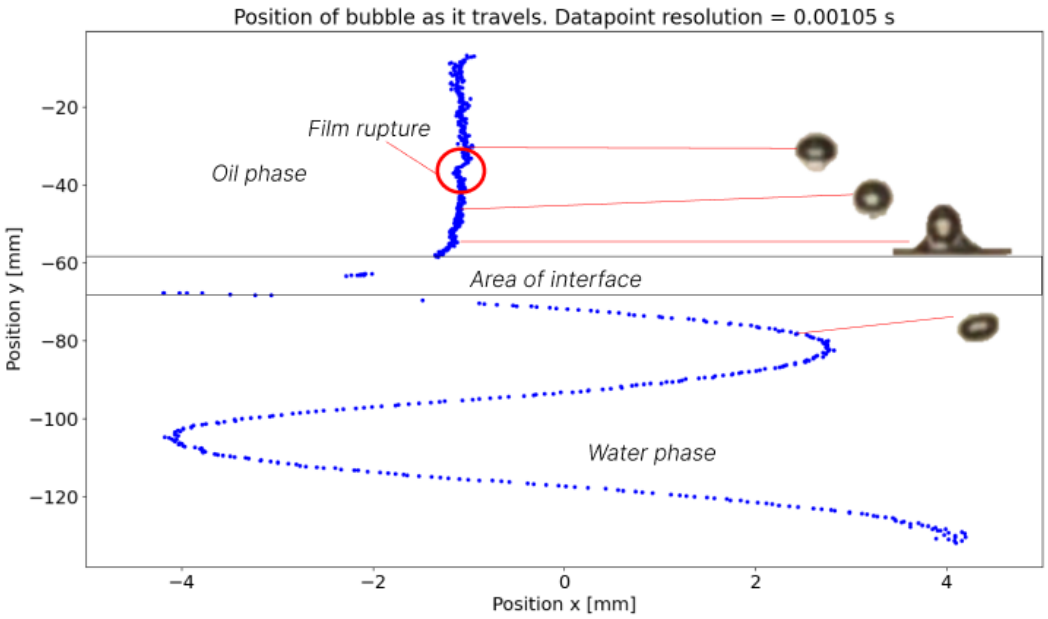

Figure 10: The path of the bubble's center mass from figure 8 and 9.

4.2.2 Resting at the interface

The bubbles seldom rested on the interface, usually they were only slowed down in the area of the interface. The smallest bubbles (0.05 ml) did rest on the interface in the zoomed out experiments, but not as much in the zoomed in experiment. Bubbles could rest for up to 0.4 s at the interface. The exact duration of bubbles resting on the interface was not possible to determine accurately.

4.2.3 Drainage and film rupture

The drainage behaviour has been studied with close-ups of the bubble passing the interface. When the bubble hits the interface the speed is greatly reduced due to the interfacial tension. The interface deforms in a diameter of about 3x the diameter of the bubble. The heavy phase is drawn into the light phase and a necking of the column can be observed until the surface tension of the heavy phase breaks the column. The column splits into one or more droplets above the interface, while the bubble draws the rest of the heavy phase like a tail behind itself. The larger the bubble, the more heavy phase is drawn into the light phase. When the heavy phase forms a tail behind the bubble it

seems like the film ruptures around the bubble and it is allowed to "slide out of" the heavy phase and into the light phase. This phenomena has occurred for all the bubble sizes used in these experiments. The smaller the bubble, the longer it travels before this happens, indeed the largest bubbles exhibit this behaviour as the heavy phase column is necking. In the case of the larger bubbles, the heavy phase drains so quickly that when the TPCL reaches the bottom of the bubble, a burst of heavy phase may penetrate through the bubble and come out on top of it, as seen in figure 11. Also notice the micro bubbles that are resting on the interface. These bubbles are surrounded by the light liquid, confirming that the spreading parameter is positive for the oil, and negative for the bubble and the water.

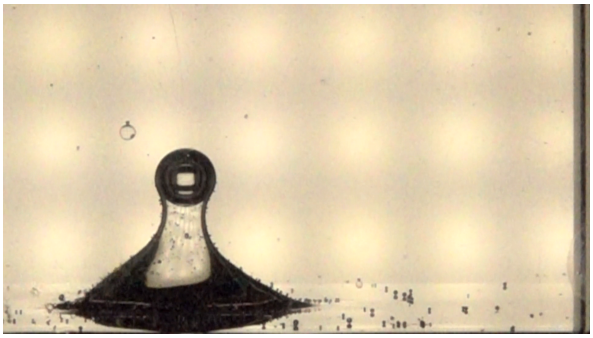

(a) 0 s. Water film covering bubble

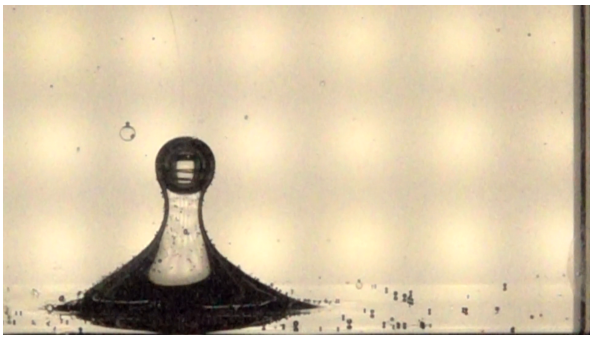

(b) 0.0083 s. Water film is drained about halfway down the bubble

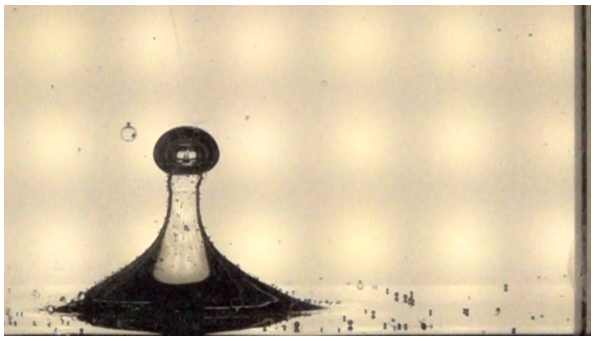

(c) 0.0156 s. A burst of water is visible within the bubble

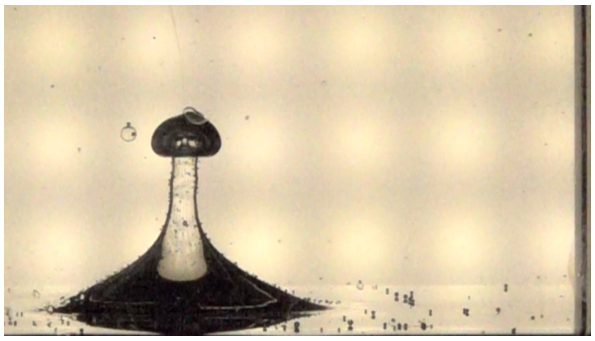

(d) 0.0240 s. Water burst has penetrated the bubble and has formed a droplet at the top

Figure 11: Water penetrating a 0.2 ml bubble while draining. Total duration = 0.024 s.

Even the 0.05 ml bubbles displayed similar a behaviour, although not as dramatic.

The water jet does not penetrate the bubble, but a droplet of water is formed inside it which then falls back down as the bubble is rising. This was very unexpected, as the 0.05 ml bubbles had not had any film ruptures in any of the three previous experiments. In figure 12 the gliding average velocity of this bubble is presented. Notice the distinct uptick in velocity around 0.32 seconds, this was the moment of film rupture.

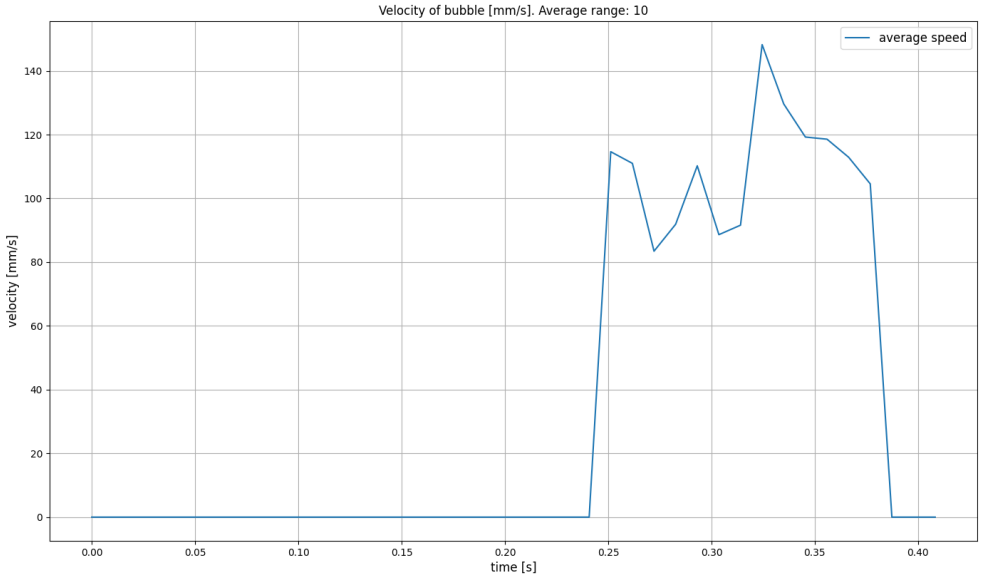

Figure 12: Gliding average velocity of 0.05 bubble in close up experiment.

There is no occurrence of water detachment from the wake in the close ups, it has however been observed in the zoomed out experiments where the bubble size is 0.15 ml or more, with a long light liquid zone. In the case of food coloring in the water, the 0.10 ml bubbles also shed the tail on it's way up. As the density difference between the heavy and light liquid phases is low, the water that detaches from the bubble wake stays suspended in the oil for extended periods.

The maximum drag forces consistently rise by a factor of between 40 and 50 when the bubbles pass into the oil, as calculated by both Stokes law 7 and equations 4 - 6. This is generally due to the extreme lowering of the Reynolds number as the viscosity rises with a similar factor. Thus this becomes an additional force that the water film

has to withstand in order to stay attached to the bubble as it rises.

4.3 Threshold values

The dimensionless parameters of Edrisi et al. [1] and the threshold values of Conochie and Robertson (as reported by Kobayashi)[9] are presented in table 3.

Table 3: Dimensionless parameters and stability parameters of performed experiments.

Bubble size [ml]	π_1	π_2	π_3	X	Y	Z
0.05	0.18258	0.00104	0.85664	0.265	0.517	0.218
0.10	0.11502	0.00073				
0.15	0.08778	0.0006				
0.20	0.07246	0.00052				

As predicted by Edrisi et al. [1] and Greene et al. [8] the 0.05 ml bubble should not be able to pass the interface, but without exception they have passed on in these experiments. In some cases they have had significant rest times before passing through. In the close-up videos all bubble sizes exhibit some form of film rupture. The water film drains off the bubble as it rises, and the water films releases the bubble without bursting into smaller droplets. The implications of the X-value in the table is that the water film around the bubble is unstable, and will at some point rupture. The Y-parameter is in such a range that dispersion of the fluids will occur. The Z-parameter implies that there will be no flotation occurring.

4.3.1 New threshold values

Keep in mind that since some of the dimensionless numbers require a velocity, and there is uncertainty in what velocities previous workers have observed, the numbers with velocity as a variable are speculative. With the input of 148 mm/s as a velocity for Edrisi et al.s [1] 2 ml bubble the dimensionless groups and group pairings are presented in table 4. Table 5 postulates that the velocity for Edrisi et al.s 2 ml bubbles is 70 mm/s, like the bubbles they have presented the velocity of (0.15 ml and 0.08 ml).

Table 4: Promising dimensionles parameters by a 2D analysis with different margins

Margin variance (+/- %)	Edrisi 2ml (v=148 mm/s) vs our 0.05 ml (v=100 mm/s)
10	π_2 ·Eo, π_8 · π_{13}, π_3 /Fe, Ar/Ga, π_1/π_{12}
25	Fr, Ca· κ_2, Fr· π_2 ·Eo, Re· π_2 ·Eo, Re· π_4 , π_3 ·Eo· π_2
50	π_3 , π_1 ·Eo, π_2 ·Eo, π_2 ·We, π_3 ·Ca/Oh, Eo· π_1, Eo· π_{12}, We·Eo· π_2 , π_7 ·Eo/Oh, π_1 · π_2
75	Ca/Oh, κ_1·Re, π_7 /Oh· π_8 , Ca· π_3 /(Fr·Oh), Ca·Ar/(Oh·Ga), Re·Oh, We·Fr, We· π_3 , π_8 · π_2 , π_8 · π_{12}, π_8 · π_1, π_3 ·Fr , π_3 ·We, π_1/π_{13}, π_2 /π_{13}, π_4 / π_7 , π_6 / π_7 , π_8 /Eo, Ca/Oh, Oh/ π_4 , Oh/ π_6 , Eo · OH/Ca, We/Eo, Re/ κ_2, Ca/(π_3 ·Oh), Ca/(Fr·Oh), Ca · Fr /(π_3 Oh),

Table 5: Promising dimensionles parameters by a 2D analysis with different margins

Margin variance (+/- %)	Edrisi 2ml (v=70 mm/s) vs our 0.05 ml (v=100 mm/s)
10	We, π_2 ·Eo, π_7 ·Re, Ca·Re, Oh·Re, Ar/Ga, Ca/Oh, π_7 /Oh, π_7 /Ca
25	π_3 · π_2 ·Eo, We/ π_3 , Ca/(Oh· π_3), π_7 /(Oh· π_3),
50	π_3 , π_1 ·Eo, π_3 ·We, Re· κ_1, π_1/ π_2 , π_4 / π_6 ,
75	π_3/Fr, π_1 · π_8 , π_2 · π_8 , Eo·Fr, π_8 /Eo, Ca/ π_4 , Ca/ π_6 , Oh/ π_4 , Oh/ π_6 , Fr/ π_1 , Fr/ π_2

4.4 The food coloring debacle

There was no experiment performed to explicitly study the effect of surfactants on the system. However, when attempting to improve the image processing food coloring was added to the water. This left the interface with many droplets and bubbles that would not coalesce. Both the water column and entrained water contracted differently than in the experiments without food coloring. A part of the videos (0.75 s after the bubble enters the chamber) is presented in figure 13.

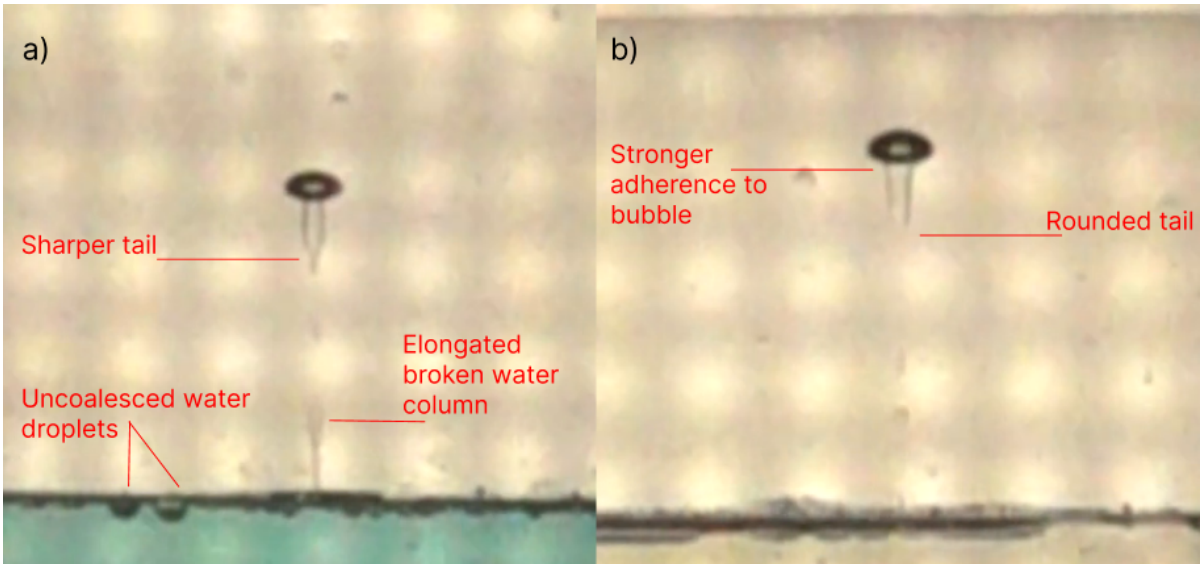

Figure 13: A comparison of the 0.15 ml bubbles in food colored water (a), and normal tapwater (b).

In the images above it is possible to see the unusual shapes of the water tail beneath the bubble. The entrained water is more elongated and sharper than in the case of the non contaminated water. Also notice the higher amount of droplets on the interface. The interface was cleaned before the experiments were performed, but the food colored water was harder to clean than the normal tapwater. The adherence of water to the bubble seem to be stronger for the non food colored water. The angle between the water and bubble is more rounded and has a larger area in contact with the bubble than in the case of the food colored water. The velocity does not seem to be lower compared to the non food colored water. Figure 14 is the measured velocity of the 0.10 ml bubble in food colored water, which can be compared to the non food colored velocity graph in figure 8.

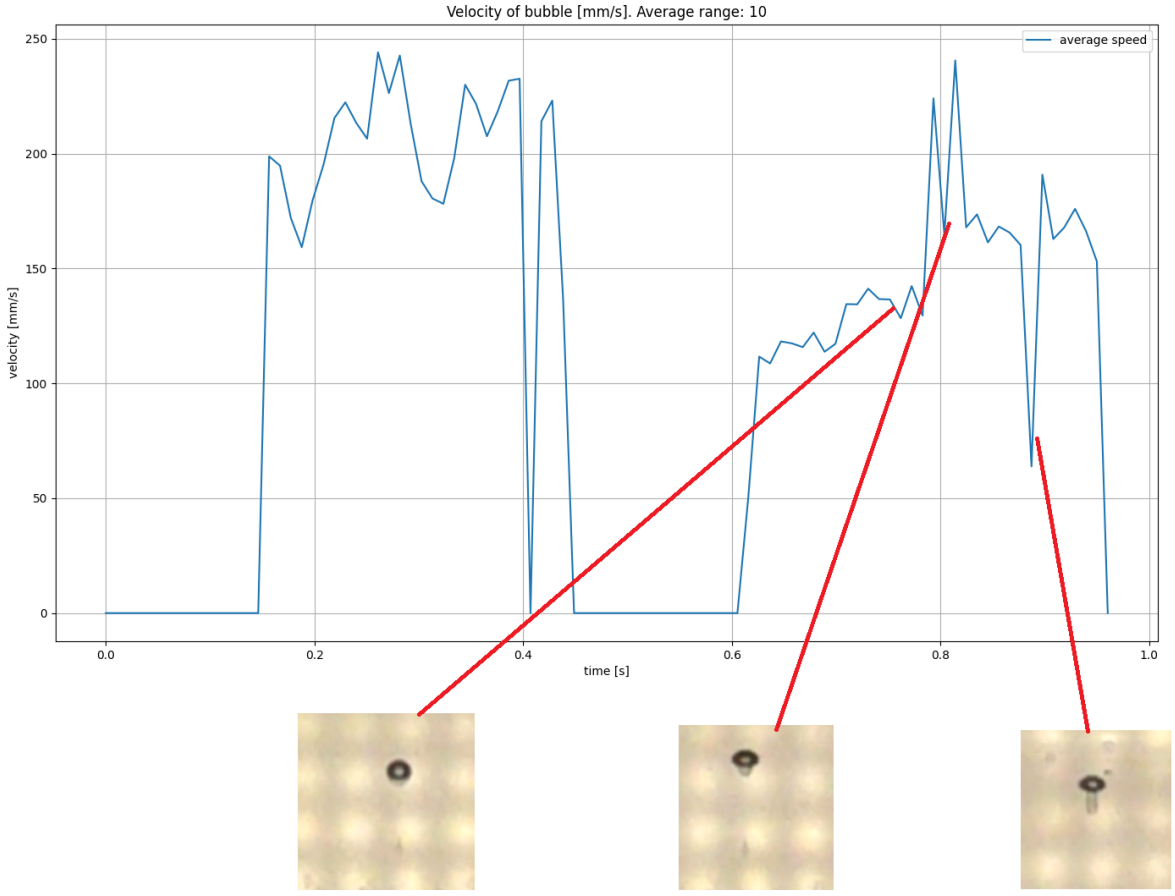

Figure 14: 10-point gliding average velocity of 0.10 ml bubble in food colored water. Bubble behaviour at anomalous velocities are also visible.

Compared to the non-colored water the bubble in this graph seems to have just as high velocities. The point at which the film ruptures seems to be at roughly the same point as in the case of the non-colored water, at about 0.8 s. The reason for the spike is the sudden shift in bubble shape from spherical to ellipsoidal, so that its center mass is moved rapidly upwards. The interesting dip in the velocity at about 0.9 seconds is the point where the entrained water detaches from the wake of the bubble and eventually falls off. Recall from figure 8 that a similar dip is not observed in the upwards velocity, and indeed the bubble does not shed the entrained water tail in that case either. Such behaviour was not only observed in the food color contaminated system (with a bubble volume of 0.10 ml and up), but also in the systems without food coloring from 0.15 ml

and 0.20 ml. The dip at 0.4 seconds is due to incompleteness of data points in that region.

When the entrained water detached from the bubble it would only form spherical droplets if the volume of water was large enough. As can be seen in figure 15, there are three droplets formed in the wake of the bubble where only the largest one contracted into a sphere.

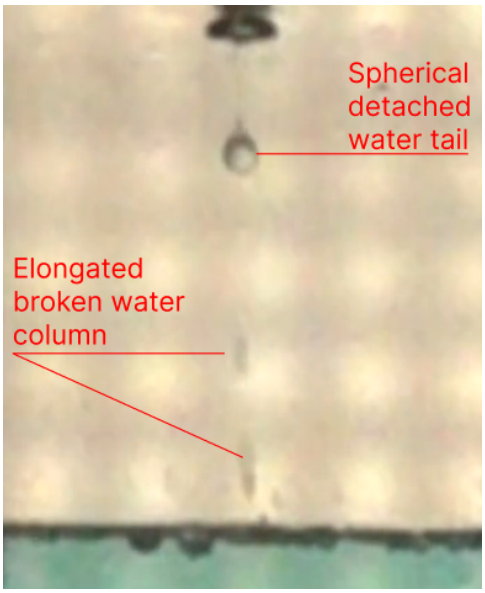

Figure 15: Fully detached water from 0.20 ml bubble in food colored water.

The shape of the different bubble sizes are presented in figure 16.

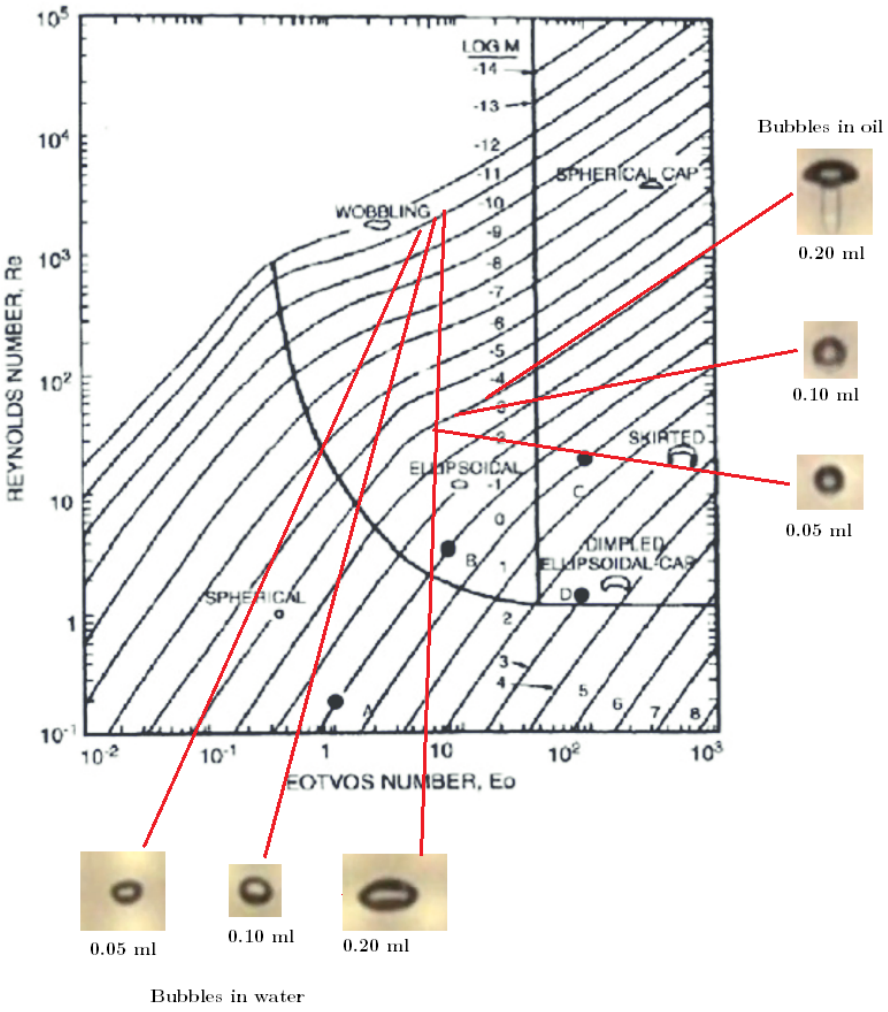

Figure 16: The shapes of the bubbles in water and in oil

5 Discussion

5.1 Film rupture

As is seen in the close up videos, the film drains off the largest bubbles even before the water column breaks. The film rupture is contained to a single large drop, which is not typically reported in the literature. Two properties are suspected to play a role in this regard, namely the viscosity and the surface tension. The surface tension in these experiments are lower than what has been used by for example Edrisi et al. [1], and they got a much more dispersed film rupture than what has been observed here. However, as the literature typically reports that a lower interfacial tension leads to a larger number of dispersed droplets from the film rupture, it seems like there are other factors playing in here too. The viscosity of the oil is a probable culprit, as the property governs the dissipation of kinetic energy in a liquid. Thus, the resistance to breaking apart and forming numerous smaller droplets may be nigh impossible due to the resistance to flow of the oil.

The burst of water into the bubbles as the film drains off is an interesting case as well. In the case of the 0.15 and 0.20 ml bubbles a small amount of water was ejected out on the top of the bubble within the time span of 0.03 seconds. This phenomenon was not found in the literature, although the mechanism seems similar to droplet ejection when a water drop hits and deforms a water surface which then ejects a jet and a droplet when the surface contracts back towards water level. Since the surface tension and hydrostatic pressure is responsible for this contraction in the case of water-air interfaces, it is believed that the high density of the oil, and as such the pressure it exerts on the water, also plays a role in this phenomena in the case of a water jet within the bubbles. It would be interesting to perform experiments with different densities of the water compared to the oil in order to see where the threshold for this behavior lies, however, finding a product that is soluble in water and not the oil could not be done for this project. The viscosity of the water is a resistive force to the water jet. It is thus believed that the phenomenon can be described by the ratio of hydrostatic and interfacial tension forces to viscous forces.

5.2 Bouncing on the interface

The phenomenon of bubbles bouncing and being arrested on the interface was not observed in any experiments. The smallest bubbles seemed to rest for some time before passing into the oil, though. As stated earlier, this is contrary to what has been found

by previous work. It was expected that the 0.05 ml bubbles would not pass the interface.

5.3 The effect of surfactants

When food coloring was added to the water, the velocity of the bubble did not seem unaffected. However, it still travelled upwards at the same rate as in the case of the non-contaminated experiments. This is somewhat perplexing, as the litterature reports that the velocities of bubbles with diameter in the order of magnitude of 1-10 mm is strongly affected by surfactants. The bubbles in these experiments have an equivalent diameter of around 5 mm, and as such should be strongly affected by this. Since no experiments have been performed to assess the influence of surfactants on the system, it is not known whether or not the concentration was high enough to get a significant reduction in bubble velocity.

The effect on the entrainment of water was more readily visible. As the bubble was rising, the water that was drawn into the oil did not form spheres unless the volume of water was significantly high. This may be due to the interface becoming more rigid as the surfactants "bridge" the properties of the water, the oil and the air in the phase boundary, which combined with the high viscosity of the oil may resist the formation of spherical droplets. Although the droplets detaches from the bubbles in the cases of 0.10 ml and up, it is not known how beneficial this is to retain phase separation. As the interface is more rigid and the non polar part of the interface is going outwards in the case of water, there is a higher resistance for the droplets to rejoin the water phase compared to a non contaminated system. It is possible to get a lot of water droplets on the oil-water interface that simply will not coalesce into the water phase. This may be counteracted with a higher density difference between the two liquids though, as there will be more gravitational forces acting downwards on the heavy phase and thus facilitate a breach at the interface of the resting drops.

Interestingly the 0.05 ml bubbles only experienced a film rupture in the close up experiments. This may be due to a thorough cleaning of the test chamber with soap followed by ethanol and finally some isopropanol. As such this may be the least surfactant contaminated experiment of them all. Since surfactants lowers the interfacial tension and renders the interface between these liquids more rigid, the surface tension forces may be more free to contract the entrained water in cleaner systems. With a lower interfacial tension than what has been measured in clean systems, the rupture may be facilitated by the trace presence of surfactants. The drag from the viscous oil is probably further facilitating the film rupture.

Another interesting point is that the 0.05 ml bubbles spent more time resting on the interface in the first experiments and especially in the food color contaminated experiments than on the last close-up experiments. This may point towards surfactants being both capable of inducing and reducing behaviours depending on the concentration of them. Very low concentrations makes the surface- and interfacial tension forces more prominent in the behaviour, while at higher concentrations these forces are less influential, but drag becomes more significant when the interface is more rigid.

As can be seen in figure 13 the water seems to adhere less to the bubble in the food colored experiment. The reason for this may be higher drag caused by the rigid interface and elongated tail of entrained water, leading to more forces acting on it. Due to the lower surface tension, the water could be expected to adhere more strongly to the bubble though. Indeed both of these effect may play a role, but the drag increase is a more influential factor. As the effect of surfactants are experienced on several fronts it is hard to conclude on anything without deliberate experimentation.

5.4 The effect of drag on the entrained water

The drag forces experienced by the bubbles are drastically changing when they leave the water and enters the oil. As calculated by equations 3 to 7 for a spherical bubble without entrained water the drag force is between 40 and 50x higher in the oil than in the water. Whereas this may not be entirely correct when the bubble is rising after the film has ruptured, the shape of the bubbles and entrained water before the film ruptures is spherical as can be seen in figures 11 and 14. It is believed that this drag is a very influencing factor in the film drainage, as it is reported in the literature that a higher viscosity leads to a more rapid film drainage. Interestingly, in the case for Edrisi et al. [1] the drag force coefficient would decrease drastically when the bubble enters the light phase, which was hexane. Since the drag increase with the inverse of the Reynolds number, a higher viscosity will usually be the most influential contributor to an increase in drag.

As the effect of viscosity in the light phase seems highly influential in the film drainage and -rupture, it should be represented in the dimensionless numbers for the film rupture. However, since no bubble size has been identified to reliably not experience film rupture a threshold value cannot be confidently set. As the 0.05 ml bubbles are not experiencing a film rupture in the uncleaned experiments, the threshold value for this phenomenon is probably very close to the case of the 0.05 ml bubbles.

5.5 The effect of buoyancy around the interface

The buoyancy effect is the strongest single force in these systems, as the bubbles invariably rises. An interesting aspect of buoyancy is that the force scales linearly with the density of the surrounding fluid that a body displaces. As these experiments contains more than one liquid medium for the bubbles to traverse, there are two different buoyancy situations for the bubble. Consider the case of the bubble being above the liquid-liquid interface, but fully covered in the heavy liquid, as seen in figure 11a. In this case the bubble are affected by all the forces of the system: surface tension, gravity, interfacial tension, buoyancy and drag are represented. Interestingly, the bubble is now affected by the buoyancy of the oil, which is 85 % of the density of the water below. As such there is a very small reduction in buoyancy forces. If the interfacial tensions and drag forces are sufficiently high here, the bubble may not be able to get enough forces acting upwards to actually breach the interface. As such the density difference between the two liquids can be of critical importance in stopping bubbles from passing the liquid-liquid interface. Regrettably, only one oil was used as the light phase in these experiments, and the density difference between them could not be manipulated to yield threshold values for the effect of buoyancy.

5.6 Comparison to threshold values

Edrisi et al. [1] used a water-hexane system with a test rig that this thesis has been inspired by. The water-hexane system has a higher interfacial tension than the water-oil combination that is studied here. The viscosity of the hexane is significantly lower than the oil used in this thesis. As a sidenote, they have also published videos from their experiments, which have been very illustrative of their findings.

The dimensionless parameters they introduced as presented in equations 24 to 26 have been used to evaluate the results from this thesis as well. However, when calculating the threshold values, different results were found for π_2. The error was not found, but the threshold value should be 8.2107e-4 for bouncing on the interface, and 1.6421e-4 for film rupture with a water viscosity of 1.002 mPa s and bubble sizes of 0.08 ml and 2 ml respectively. Also π_3 seems to be very off, as the density of air would need to be 1374 kg/m^3 in order to get a value of 1.93721. This density is 1000x higher than what is typically reported, and as such it is assumed that it should be 1/1000 of this value. Then we get a threshold value of 0.65951.

With these new threshold values the experiments performed for this thesis can be

more closely compared. As has been stated, there was no volume of bubbles that did not pass the interface, and as such these threshold values seem to miss something important. The main differences between Edrisi's experiments and the experiments performed here is the the viscosity of the oil, the density difference between the liquid phases and the surface- and interfacial tensions. While Edrisi et al. [1] needed 2 ml bubbles in order to get a film rupture, the experiments performed here experience film ruptures down to 0.05 ml, and without dispersion of smaller droplets as in the case of Edrisi et al.'s [1] experiments. The reason for the early film ruptures here may be a lower interfacial tension combined with increased drag from the oil's viscosity and the low density difference. The lower density difference exerts a higher pressure on the bubble film when entering the oil as compared to the lower density hexane used by Edrisi et al. [1].

Using the threshold values may not be completely currant here, since in the cases of the 0.05 ml bubbles the film rupture did not happen on the "unclean" experiments, and as such the surface- and interfacial tension values may be off compared to the close up experiment. The bouncing or arresting of the bubble on the interface was not observed in these experiments either.

5.6.1 Bubble bouncing on interface

According to the penetration condition by Greene et al. [8] and Edrisi et al. [1]. as presented in equation 32, the smallest volume of bubble that should be able to penetrate the interface in the performed experiments is 0.057 ml. Since the 0.05 ml bubbles managed to penetrate it without fail, there seems to be some discrepancy in either the actual volume of the bubbles or in the equation. The volume of the bubbles was not performed as accurately as in the case for Edrisi et al. [1] due to issues regarding the syringe sizes in these experiments. However, due to the way they were delivered the bubble size should only be smaller than the measured volume, as the intrusion of water into the syringe tip was an issue in some cases. The syringes were in the range of 0.5 ml, with markings for every 0.05 ml and as such, it could be confidently disregarded as a major source of error. The surface- and interfacial tension has been suspected to veer off from the expected value. The trace presence of surfactants may be an issue in both the experiments performed here as well as for Edrisi et al. [1]. Another possible contribution is the change in buoyancy forces as the bubble passes into the lighter phase. In the experiments performed here, water has only 17% higher density than the oil, and as such the strongest single force in the system does not decrease as much as with a hexane

system, where the water has about 50% higher density. Since the buoyancy forces scale linearly with the density of the surrounding fluid, this may be a contributor in arresting the air bubbles on the interface. As the bubble rises with the intact water column and displaces the light phase, the sudden reduction of buoyancy forces (50% in the case of hexane) could be instrumental in arresting the bubbles on the interface. As such it may be worthwhile to implement the effect of the density difference in a new dimensionless parameter.

5.6.2 Film rupture

For the 0.05 ml bubble in the theoretically cleanest experiment the obtained values for π_1, π_2 and π_3 is 0.18258, 0.00104 and 0.85664 respectively. These would be the threshold values for which the film will rupture. If they are larger (at least the first two), the film should not rupture. In the case of the interfacial tension, only π_1 is affected by the change in interfacial tension, and as such this is probably the critical parameter that could be subject to change.

Due to what has been observed in these experiments, and what has been discussed section 5.4, another dimensionless threshold value should be introduced. The effect of the drag increase in the heavy phase seems to be of such importance to the film drainage and -rupture that it must be considered. Since the dimensionless number π_2 (equation 25) takes the viscosity of the heavy phase into account, it does not give a good indication on the changing flow conditions of the light fluid. As such it is believed π_2 is a suitable description for the "bouncing on interface"-phenomenon, but not for the film rupture in light liquid. A very simple fix would be to introduce π_4, as previously defined in equation 39. This equation is exactly the same as π_2 in equation 25, but with the properties of the light liquid instead of the heavy liquid. It represents the drag forces to the buoyancy in the light liquid.

Although the implementation of π_4 seems like a simple correction, it is insufficient for the evaluation. The 0.05 ml bubble did in one case experience a film rupture, which was probably due to the low amount of surfactants in the system. As such, the interfacial tensions are probably just as influential. With π_4 the threshold value for film rupture lies in the range above 0.06861 for the experiments performed in this thesis. The exact number is not possible to validate with the current experiments and experimental setup. The experiments performed by Edrisi et al. [1] would have a π_4-threshold value at 7e-5. Had it not been for the order of magnitude difference, this would be promising.

5.6.3 New dimensionless groups

With a variance of 10% from unity between the experiments performed here and in previous reports like Edrisi et al. [1] of the dimensionless groups, the numbers with the most promise for describing the film rupture phenomena has been found. One of the most interesting parameters is $\pi_2 \cdot Eo$. This parameter reduces to equation 50.

$$\pi_2 \cdot Eo = \frac{\mu_2}{\sigma_{12}} \left(\frac{\rho_1 - \rho_b}{\rho_2 - \rho_b} \right) \frac{g d_b^2}{\sqrt{g d_b^3}} \tag{50}$$

Although this seems like it contains most of the necessary parameters, it does not contain the viscosity of the light liquid, which has been reported to be one of the most influential factors on film rupture. It does however capture the changing buoyancy effects that has been discussed earlier. Another strength of this parameter is that it does not contain any velocity terms, which can be very hard to acquire measurements of. For this formula the threshold value is 4.8723e-3

With the assumption that the terminal velocity of the bubbles in Edrisi et al.s experiment is roughly equal to their 0.08, and 0.15 ml a new ratio of two dimensionless numbers show up. The Capillary number (equation 28) divided by the Ohnesorge number (equation 29) could be of interest. It reduces to equation 51.

$$Ca/Oh = \frac{u\sqrt{d_b \rho_1}}{\sqrt{\sigma_{12}}} \tag{51}$$

As can be seen, many of the properties that are relevant to the problem are represented in this equation. It is somewhat reminiscent of the Weber number. The lack of μ_1 is due to it appearing as a numerator in both the dimensionless numbers. The seeming disappearance of a property that has been identified as key to drainage and rupture is somewhat concerning though. The fact that the weight of the entrained water is not present in this is also sub-optimal. . With this parameter the threshold value is 1.0236.

π_7 (equation 42 can be of interest as well. Divided with either the Capillary or the Ohnesorge number it is within 10% of unity for the compared experiments. The reduced equation is presented in 52.

$$\pi_7/Oh = \frac{\sigma_{12}^{3/2}}{\rho_1^{1/2} u^3 d_b^{3/2}} \tag{52}$$

Once again μ_1 appears as a numerator in both numbers (the same applies to π_7/Ca). Having both the velocity and diameter of the bubble as inputs is not necessarily a negative, but ideally only one should be needed to describe the threshold values. With this equation the threshold value is 6.0302e2.

Another interesting candidate is $Re \cdot \pi_7$, which reduces to equation 53.

$$Re \cdot \pi_7 = \frac{\sigma_{12}}{\rho_1 u^2 d_b} \tag{53}$$

This is the inverse Weber number, which will be discussed later.

If the terminal velocity is closer to 148 mm/s, the π_3/Fr shows up as a candidate. This number reduces to equation 54.

$$\pi_3/Fr = \frac{(\rho_1 - \rho_b) \cdot \sqrt{g d_b}}{(\rho_2 - \rho_b) \cdot u} \tag{54}$$

This captures the buoyancy effects, the velocity and the size of the bubble. It does not have any viscosity, or interfacial tensions, and as such, it seems more like a coincidence that the experiments have this parameter in common. The threshold value is 1.814.

It should once again be stated that the terminal velocity of previous works is not known. However, with what has been calculated for the bubbles in the experiments performed here, the bubbles are estimated to be twice as fast as what is observed. If this is true for the experiments of previous works as well, the 148 mm/s could be twice as high as what has been observed in those experiments as well. Thus roughly 70 mm/s has been speculated to be a low end terminal velocity of the previous work.

It also seems like in both cases of terminal velocity estimation of previous works the numbers π_1/π_2 is within 50% of unity. This is reduced to equation 55.

$$\pi_1/\pi_2 = \frac{\sigma_{12}\sqrt{d_b^3}}{\mu_2 d_b} \tag{55}$$

The threshold for this value is 5.9394 by the experiments of Edrisi et al [1]. However, it predicts that the 0.05 ml bubbles studied here are too small to experience a film rupture.

The Weber number holds similar values between the experiments, with the assumption of slow bubbles for the experiments of Edrisi et al. [1]. In this case, with the

interfacial tension as the σ-value. Since it is a measure of drag forces to cohesive forces it is an interesting parameter to study. With reports stating that the viscosity (and consequently the drag force) of the light liquid is a critical parameter of the film drainage and -rupture, the Weber number should be a good descriptor of the case, in theory. Although the viscosity does not show up explicitly in the Weber number, it can also be expressed with the drag coefficient, which is a function of the Reynolds number, and thus the viscosity is represented. The bubbles have an extremely high acceleration after passing the interface as well, as seen in figure 12 the velocity has already peaked when imageJ starts to recognize the bubbles passing the interface. As such this dimensionless group may be applicable to the problem, given that the terminal velocity is known. The threshold value is 1.0477.

5.7 Applicability to metal industry

As pointed out in different parts of the steel industry, cold models are hard to scale to a full size metal operation. The report by Tsukaguchi et al. [4] attempted to describe the ways one could use a cold(er) model in order to simulate a case in an industrial scale operation. In the findings, water seems to be applicable as a model for steel at its melting point, when the temperature of water reaches 373 K. In these experiments the temperature was 293 K, and as such it does not seem to be scaleable to steel. In any case, since the properties of the metal product and the slag is more well known by the relevant process operators, the similitude should be assessed by the interested party.

6 Conclusion

6.1 Film rupture and water jet observation

Film rupture occurred on much smaller bubbles than what was expected. According to previous work, the bubbles should not experience a film rupture until the bubble size was 1.3 ml. However, even the 0.05 ml bubbles studied here experienced a film rupture. The reason for the discrepancy is suspected to be a failing to consider the viscosity of the light liquid as an influential factor on the phenomenon.

A jet of water that formed inside the bubbles as the film ruptured was also observed. While not especially significant for the purposes of this thesis, the phenomenon was interesting to observe. It is suspected to be easily described very similarly to how water jet columns forms when a water droplet falls unto a water surface.

6.2 Threshold values

No definitive threshold value could be confidently presented due to the limited range of bubble sizes and that entrainment and film rupture was observed on all bubble sizes. Film rupture was the only phenomena where a threshold could be determined. The Weber number could be of interest in this regard based on the fact that it is a measure of drag forces to cohesive forces. As previous work has determined dynamic viscosity (and by extension; drag forces) as a property that affects film drainage and -rupture, the Weber number seems fitting. The threshold value for this is 1.0460 for film rupture. The capillary number divided by the Ohnesorge number may be a viable candidate, with a threshold value of 1.0236. Finally $\pi_2 \cdot Eo$ could also be of use, with a threshold value of 4.8723e-3.

A threshold value for bouncing on the interface, heavy liquid entrainment and satellite formation was not determined, as all bubble experiments performed here passed through the interface, entrained water, and did not fulfill the precursors for satellite formation.

6.3 Applicability

The interested parties should assess the applicability of the found results. The report of Tsukaguchi et al. [4] can serve this purpose.

6.4 Further work

It is suggested that further work is done by using several different liquids to obtain threshold values. A better setup, which could accommodate both larger and smaller bubble sizes should also be employed. Smaller bubbles than what was obtained here should be produced to find the exact threshold value.

The phenomena of a water jet inside the bubbles could be interesting to study further. This behaviour is, at least to the author's knowledge, not entirely described.

References

[1] A. Edrisi, M. Dadvar, and B. Dabir, "A novel experimental procedure to measure interfacial tension based on dynamic behavior of rising bubble through interface of two immiscible liquids," Amirkabir University of Technology, Tehran, Tehran, Iran, Tech. Rep., 2021.

[2] S. Bublik, J. E. Olsen, V. Loomba, Q. G. Reynolds, and K. E. Einarsrud, "A review of ferroally tapping models," Norwegian University of Science and Technology (NTNU), 7491 Trondheim, Tech. Rep., 2021.

[3] R. Clift, J. R. Grace, and M. E. Weber, *Bubbles, Drops and Particles*. 111 Fifth Avenue, New York: Academic Press, 1978.

[4] Y. Tsukaguchi, K. Fujita, H. Muramaki, and R. I. L. Guthrie, "Physical modelling for the precise representation of flow phenomena based on simultaneous similitude of multiple dimensionless numbers," Nippon Steel Corporation, McGill University, Sunayama Kamisu City and Montreal Quebec, Tech. Rep., 2021.

[5] A. Rozario, N. Viswanathan, and S. Basu, "Rise of gas bubbles across the interface between two liquids," *Metall Mater Trans B*, vol. 50, no. 1, pp. 10–15, 2019. DOI: https://doi.org/10.1007/s11663-018-1434-1.

[6] A. Rozario and S. Basu, "Physical modelling of slag foamming in presence of liquid metal phase," Indian Institute of Technology - Bombay, Mumbai, India, Tech. Rep., 2014.

[7] E. Li, S. Al-Otaibi, I. Vakarelski, and S. Thoroddsen, "Satellites during bubble transition through immiscible interface," *Journal of Fluid Mechanics*, vol. 744, no. 1, 2014. DOI: 10.1017/jfm.2014.67.

[8] G. A. Greene, J. C. Chen, and M. T. Conlin, "Onset of entrainment between immiscible liquid layers due to rising gas bubbles," *International journal Heat and Mass Transfer*, vol. 31, no. 6, pp. 1309–1317, 1988.

[9] S. Kobayashi, "Iron droplet formation due to bubbles passing through molten iron/slag interface," *ISIJ International*, vol. 33, no. 5, pp. 577–582, 1993.

[10] M. V. Berry, "The molecular mechanism of surface tension," *Physics education*, vol. 6, pp. 79–84, 1971. DOI: https://iopscience.iop.org/article/10.1088/0031-9120/6/2/001/pdf?casa_token=fr4JNAPCGsoAAAAA:VAL2uijqRQlcek6sG5gzplNkfF8t6MAdgArgtWD51o1Th1iXHlwEGBoi0F8RrJ-xHv4fm3J7v3Nvtg.

[11] M. J. Neeson, R. F. Tabor, F. Grieser, R. R. Dagastine, and D. Y. C. Chan, "Compound sessile drops," *Soft Matter*, vol. 8, no. 43, pp. 11 007–11 194, 2012. DOI: 10.1039/c2sm26637g.

[12] D. Kosior, J. Zawala, R. Todorov, D. Exerowa, and K. Malysa, "Bubble bouncing and stability of liquid films formed under dynamic and static conditions from n-octanol solutions," *Colloids and Surfaces A: Physiochemical and Engineering Aspects*, vol. 460, pp. 391–400, 2014. DOI: http://dx.doi.org/10.1016/j.colsurfa.2013.11.022.

[13] N. Pannacci *et al.*, "Equilibrium and nonequilibrium states in microfluidic double emulsions," *Physical Review Letters*, vol. 101, p. 164 502, 2008.

[14] V. Chevrier and A. W. Cramb, "Observation and measurement of bubble separation at liquid-liquid interfaces," *Steel research int.*, vol. 75, no. 10, pp. 645–658, 2004.

[15] M. J. Rosen and J. T. Kunjappu, *Surfactants and Interfacial Phenomena*. 111 River Street, Hoboken, NJ: John Wiley and Sons, 2012.

[16] Various, *Slag Atlas*. Sohnstraße 65 40237 Düsseldorf: Stahlinstitut VDEh, 1995.

[17] F. M. White, *Fluid Mechanics*. 1221 Avenue of the Americas, New York, NY: McGraw-Hill, 1999.

[18] K. E. Einarsrud, "Dimensional analysis: Lecture 1, subject: Advanced heat and mass transfer (tmt4208)," Norwegian University of Science and Technology (NTNU), 7491 Trondheim, Tech. Rep., 2020.

[19] P. E. Ramirez-Lopes, P. N. Jalali, J. Björkvall, U. Sjöström, and C. Nilsson, "Recent developments of a numerical model for continuous casting of steel: Model theory, setup and comparison to physical modelling with liquid metal," Swerea MEFOS AB and SSAB EMEA, Luleå, Sweden, Tech. Rep., 2013.

[20] C. A. Schneider, W. S. Rasband, and K. W. Eliceiri, "Nih image to imagej: 25 years of image analysis," *Nature Methods*, vol. 9, no. 7, pp. 671–675, 2012. DOI: 10.1038/nmeth.2089.

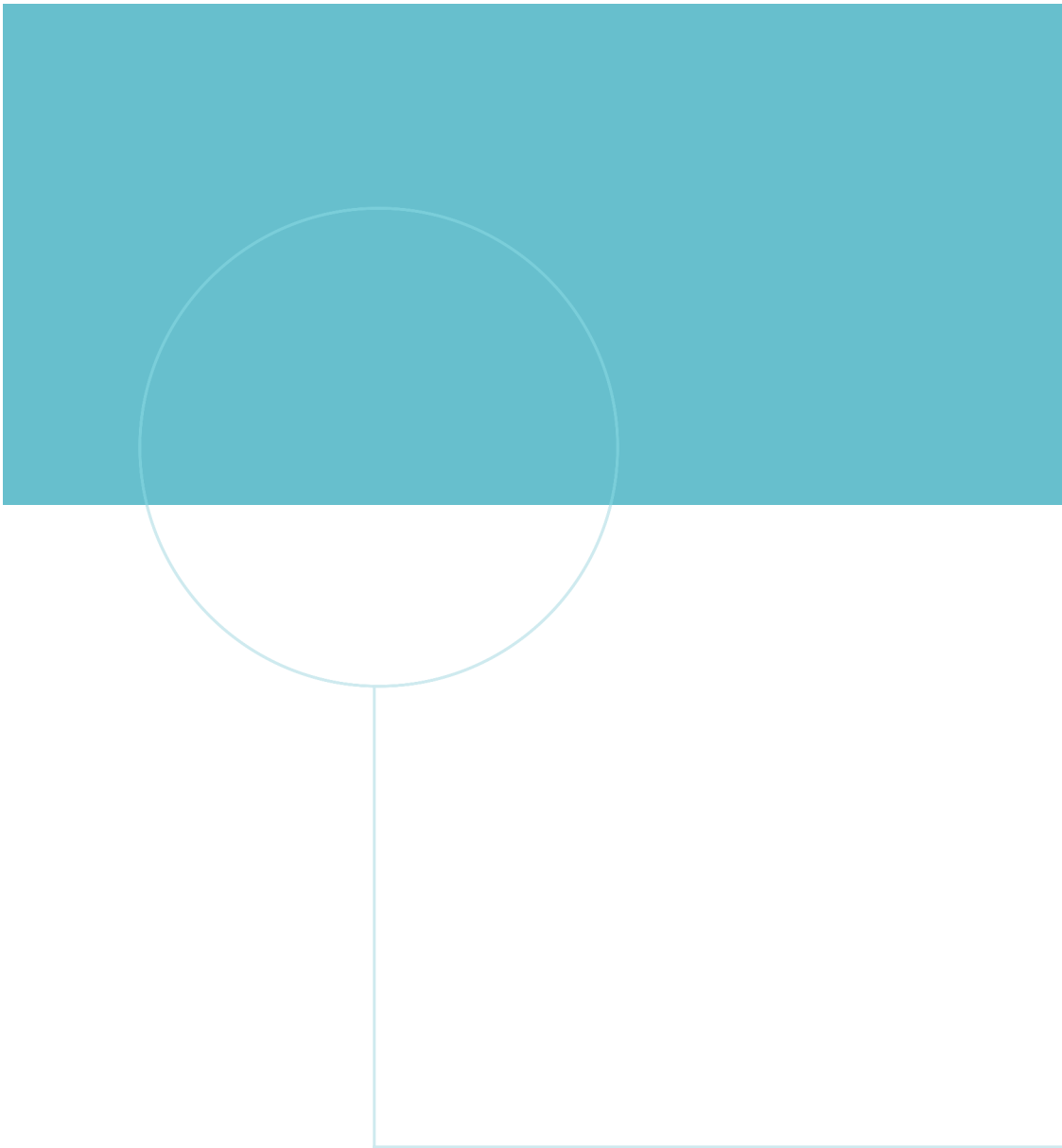

NTNU

Kunnskap for en bedre verden